

Leptogenesis Effects on the Gravitational Waves Background: Interpreting the NANOGrav Measurements and JWST Constraints on Primordial Black Holes

K. El Bourakadi^{1,*}, H. Chakir^{1,†} and M. Yu. Khlopov^{2,3,4‡}

¹*Subatomic Research and Applications Team,
Faculty of Science Ben M'sik,
Casablanca Hassan II University, Morocco*

²*Institute of Physics, Southern Federal University,
194 Stachki, Rostov-on-Donu, Russia*

³*Virtual Institute of Astroparticle Physics, 75018 Paris, France
and*

⁴*National Research Nuclear University MEPhI, 115409 Moscow, Russia*

(Dated: May 21, 2024)

We demonstrate that the leptogenesis mechanisms, which are associated with B-L symmetry breaking mechanism has notable effects on the production of gravitational waves. These gravitational waves align well with the recent observations of a stochastic gravitational wave background by NANOGrav and pulsar-timing arrays (PTAs). For these gravitational waves to match the recent measurements, the critical value of the B-L breaking should be around the GUT scale. Moreover, we consider the generation of primordial gravitational waves from binary systems of Primordial Black Holes (PBHs) which could be predicted by the recent detection of gravitational waves. PBHs with specific masses can be responsible for massive galaxy formation observed at high redshifts reported by the James Webb Space Telescope (JWST). We contemplate the potential for a shared source between the NANOGrav and JWST observations, namely primordial black holes. These black holes could serve as seeds of rapid galaxy formation, offering an explanation for the galaxies observed by JWST.

I. INTRODUCTION

Gravitational Waves Background (GWB) provides a captivating glimpse into the early stages of the universe [1]. These waves emerge either from quantum fluctuations occurring during the inflationary period [2], sourced by the phase transition of the Universe, results from cosmic strings [3, 4], or Binary Black Holes (BBH) from the early Universe [5].

During the B-L breaking phase transition ending hybrid inflation, most of the vacuum energy density gets swiftly transferred to B-L Higgs bosons in a non-relativistic state and a significant portion also goes into the formation of cosmic strings. Entropy and baryon asymmetry are produced through thermal and nonthermal leptogenesis as a result of the decay processes involving massive Higgs bosons and Majorana neutrinos [6, 7].

The operators responsible for violating the lepton (or B-L) number, emerge as a result of the exchange of massive Majorana neutrinos N_i (where $i = 1, 2, 3$) [8, 9]. When these heavy neutrinos N_i undergo decay, they inherently generate lepton (or B-L) asymmetry, assuming that the principles of C and CP conservation do not hold [8]. The resulting lepton asymmetry is then converted into baryon asymmetry during the early stages of the universe [10]. As a consequence, the process of leptogenesis appears to be the most intrinsic mechanism for explaining the observed baryon asymmetry in the current universe.

Up to this point, a range of scenarios for leptogenesis have been put forth, contingent on the methods of producing the heavy Majorana neutrinos N_i [11–14]. Of these scenarios, the most widely recognized is the conventional approach involving the thermal generation of N_i during the early phases of the universe. A comprehensive analysis [11] reveals that a satisfactory lepton asymmetry, capable of accounting for the existing baryon asymmetry can be achieved when the reheating temperature T_{re} following inflation is approximately in the range of $\mathcal{O}(10^{10})$ GeV. However, delving into leptogenesis within the context of supergravity introduces a cosmological issue concerning gravitinos: the production of an excessive number of gravitinos occurs with a T_{re} around 10^{10} GeV, to maintain the viability of big-bang nucleosynthesis (BBN) [15, 16]. To tackle this predicament, one approach is to postulate that the gravitino

* k.elbourakadi@yahoo.com

† chakir10@gmail.com

‡ khlopov@apc.in2p3.fr

serves as the lightest supersymmetry (SUSY) particle with a mass denoted as $m_{3/2}$, which falls within the range of around $(10 - 100) \text{ GeV}$ [17–20].

In this work, we calculate the gravitational wave spectrum projected by the cosmological breaking of B-L symmetry. This spectrum is influenced by various sources as enumerated earlier, including the inflationary period. Our primary focus lies in the distinctive traits of the GW spectrum attributed to binary systems of black holes originating in the early universe. Additionally, we aim to establish a relationship within the GW spectrum to the values at the phase transition of the hybrid inflation which can help identify the model parameters linked to specific characteristics in the spectrum.

Confirming the inflationary paradigm is strongly associated with the identification of relic gravitational waves (GWs), which are considered a clear and unambiguous signal. In recent studies, there has been significant progress in observational cosmology. Various collaborations, such as NANOGrav [65, 66], European PTA (EPTA)/Indian PTA (InPTA) [21, 22], and Parkes PTA (PPTA) [23], have presented compelling evidence supporting the existence of a Stochastic Gravitational Wave Background (SGWB) in the frequency range of nanohertz (nHz). While these findings are primarily attributed to astrophysical sources, it remains crucial to investigate their potential cosmological origins.

The origin of supermassive black holes (SMBHs) remains uncertain, yet numerous hypotheses have been put forth. The correlation noted earlier between the masses of black holes and the dispersion of stellar velocities can be interpreted in diverse manners, ultimately leading to the question of which came first: the host galaxy or the SMBHs [24, 25]. Thanks to the impressive capabilities of the James Webb Space Telescope (JWST), we now have the opportunity to gain a more profound understanding of the conclusion of the cosmic dark ages. To date, the JWST has successfully pinpointed numerous promising galaxy candidates situated at remarkably high redshifts [26–28]. Interestingly, within the JWST Cosmic Evolution Early Release Science (CEERS) program, a collection of massive galaxy candidates situated in the redshift range of $6.5 \lesssim z \lesssim 9.1$ has been detected. These candidates exhibit estimated stellar masses $M_* \gtrsim 109M_\odot$ (where $M_\odot = 1.99 \times 10^{30} \text{ kg}$ represents the solar mass). Notably, among these candidates, there exist six sources possessing stellar masses $M_* \gtrsim 10^{10}M_\odot$ within the redshift range of $7.4 \lesssim z \lesssim 9.1$ [29]. The investigation of primordial black holes has its roots in research conducted over five decades ago [30, 31], and in recent years, it has garnered growing attention. There are diverse underlying reasons for this renewed interest. One example is the possibility that the merging of binary PBHs could produce gravitational waves that are detectable by collaborations like LIGO/Virgo/KAGRA [32, 33]. Primordial black holes represent a compelling and inherent contender for the role of dark matter (DM) within specific mass intervals [34]. In broad terms, there exist two primary mechanisms through which PBHs can influence the formation of cosmic structures: the Poisson effect [35] and the seed effect [36, 37]. When PBHs constitute a substantial proportion of the overall dark matter content, the Poisson effect becomes prevalent across all scales. Conversely, if PBHs account for only a minor fraction of the dark matter, the seed effect dominates on smaller scales.

Observations of quasars around redshift $z \sim 6$ powered by supermassive black holes (SMBHs, with masses around $10^8M_\odot - 10^{10}M_\odot$) challenge our current understanding of early black hole formation and evolution. The JWST has revolutionized this field by enabling the study of massive black holes (MBHs, with masses around $10^6M_\odot - 10^7M_\odot$) up to redshift $z \sim 11$, thus bridging the properties of these high-redshift quasars to their progenitors. Moreover, Recent claims of a vigorously accreting massive black hole (MBH) in GN-z11, a well-known star-forming galaxy at $z \sim 10.6$, suggest it may be an active galactic nucleus (AGN). Our work in this paper aims to constrain the accretion speed and the Eddington ratio of PBHs to explain the existence of galaxies powered by these MBHs or SMBHs, thereby addressing the gap from early cosmology to current observations.

This article is organized as follows, in Sec. II we discuss the relation of Leptogenesis to the B-L symmetry-breaking mechanism, in Sec. III we introduce the physics of gravitational waves spectrum and the relation to the PTA signals in light of the B-L breaking, in Sec. IV we Match the PTA signals with gravitational waves emitted by BBH Mergers and PBH mass predicted by JWST, in Sec. V we put constraints on rapid accretion rates of PBHs to explain JWST observations AGNs and SMBHs. The last section VI is devoted to a conclusion.

II. LEPTOGENESIS FROM B-L SYMMETRY BREAKING

To illustrate the dynamics of Leptogenesis, we need to examine the B-L symmetry breaking [38, 39], the presence of baryon asymmetry in the current universe suggests that B-L violating processes had a significant impact on creating the baryon asymmetry during the early universe. The lepton number operators violating B-L symmetry originate from the interaction involving massive Majorana neutrinos N_i ($i = 1, 2, 3$) [40, 41], when C and CP are not conserved, the decays of these massive neutrinos N_i naturally give rise to B-L asymmetry. The scalar potential governing the inflaton field φ is given by

$$V(\varphi) = V_0 + V_{1l}(\varphi/\varphi_c), \quad (2.1)$$

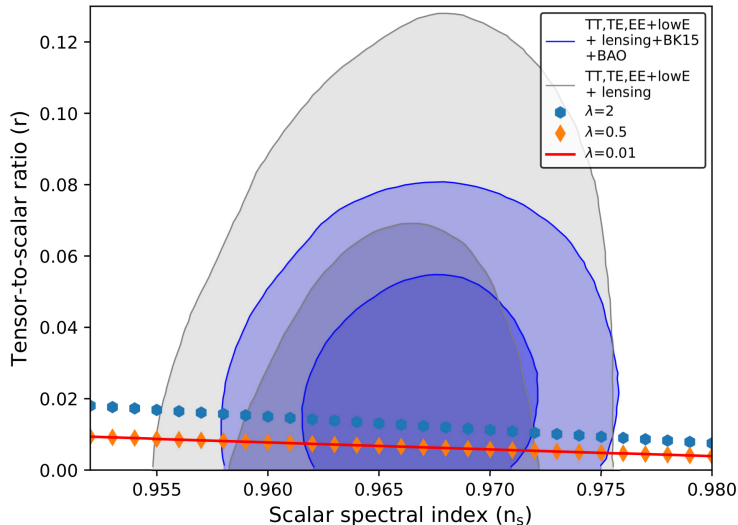


FIG. 1. r as a function of n_s for different values of λ

with $V_0 = \frac{\lambda}{4} v_{B-L}^4$ and $v_{B-L} = \varphi_c$ is the critical value of the hybrid inflation potential, for $\varphi \gg \varphi_c$

$$V_{1l}(\varphi/\varphi_c) \simeq \frac{\lambda}{32\pi^2} v_{B-L}^4. \quad (2.2)$$

When φ falls below φ_c , the B-L Higgs boson undergoes a tachyonic instability, meaning it acquires a negative mass squared. This sudden occurrence leads to the inflation coming to an end and the spontaneous breaking of B-L. The slow-roll parameters ϵ and η associated with hybrid inflation are given as follows

$$\epsilon \simeq \frac{\lambda}{16\pi^2} |\eta|, \quad (2.3)$$

$$\eta \simeq -\frac{\lambda M_p}{32\pi^3 \varphi_k^2} \simeq -\frac{1}{2N_k} \quad (2.4)$$

Considering our current study, Fig. 1 shows that the tensor-to-scalar ratio, r , shows good consistency with the predicted values of r and decreases slowly with respect to the spectral index, n_s . The results show good consistency for a wide range of model parameters with the latest observations from Planck data. Moreover, the parameter λ provide good consistency for values bounded as $\lambda \leq 0.5$ following the observational data constraints on r and n_s .

The scalar perturbations can be characterized by the curvature power spectrum, which describes the specific mode with a wave number k . When applying the slow-roll approximation, one obtains an analytical expression at the point of horizon crossing,

$$\mathcal{P}_s(k) \equiv \frac{k^3}{2\pi^2} |\mathcal{R}_k|^2 \Big|_{k \ll aH} \simeq \frac{1}{8\pi^2 \epsilon} \frac{H^2}{M_p^2} \Big|_{k=aH}, \quad (2.5)$$

here $3M_p^2 H^2 = V_0$ and \mathcal{R}_k represents the Fourier component of the comoving curvature perturbation. Similarly, the tensor perturbations $h_{\mathbf{k}}^\lambda$ can be quantified using the tensor power spectrum. By employing the slow-roll approximation, it becomes possible to derive an analytical expression for the tensor power spectrum as follows

$$\mathcal{P}_t(k) \equiv \frac{k^3}{2\pi^2} |h_{\mathbf{k}}^\lambda|^2 \Big|_{k \ll aH} \simeq \frac{2}{\pi^2} \frac{H^2}{M_p^2} \Big|_{k=aH}. \quad (2.6)$$

For both previous quantities of the power spectrum, the value of $\mathcal{P}_s \equiv \Delta_s^2$ is measured by the PLANCK satellite, $\Delta_s^2 \simeq 2.101 \times 10^{-9}$ [42], while for the tensor power spectrum $\mathcal{P}_t \equiv \Delta_t^2 = r \Delta_s^2$ [43]. One should note that, slow-roll approximated solution for the scalar power spectra enhanced scalar fluctuations, which means that small-scale

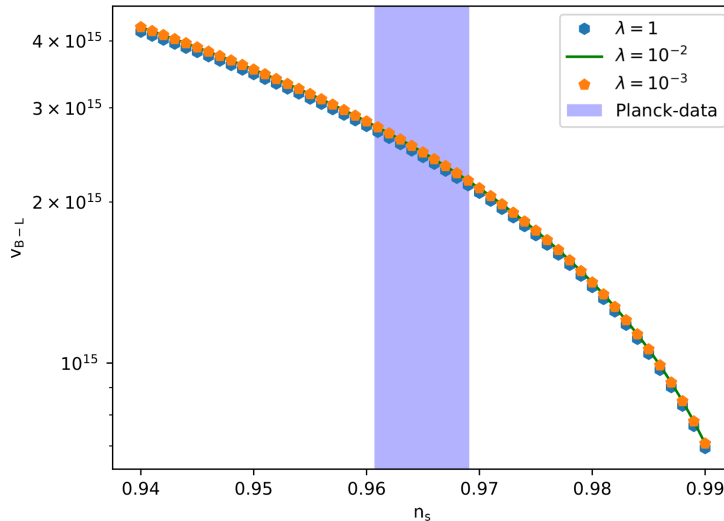


FIG. 2. Constraints on v_{B-L} according the recent Planck's bound on n_s .

fluctuations may become large enough for PBH to be overproduced. On the other hand, the tensor power spectra can act as a source for gravitational wave background.

Fig. 2 discusses the observational constraints on the critical value that leads to the B-L symmetry breaking from Planck's data, the results shows that $v_{B-L} \propto 10^{15} GeV$ and must be bounded around $\sim [2 \times 10^{15}, 5 \times 10^{15}] GeV$, our findings are also consistent with previous results [44, 45] where they proposed that the aim behind v_{B-L} value is to adjust its value to be in proximity to the GUT scale. Specifically, after conducting a thorough analysis of hybrid inflation, considering the generation of cosmic strings and non-canonical effects in the Kahler potential, the established values of v_{B-L} are consistent with all pertinent observations.

The existence of multiple heavy Majorana neutrino species (N_i) leads to two mechanisms that reduce the current lepton asymmetry. In previous findings (Ref. [45]) they considered a normal hierarchy of the right-handed neutrinos, where the most significant contribution to these processes come from the lightest right-handed neutrino (N_1), which leads to the fact that the time evolution of the reheating process is primarily governed by two key factors: Γ_S^0 and $\Gamma_{N_1}^0$. These quantities represent the vacuum decay rate of the B-L Higgs bosons and their superpartners, as well as the vacuum decay rate of the heavy (s)neutrinos belonging to the first-generation [45].

$$\Gamma_S^0 = \frac{m_S}{32} \left(\frac{M_1}{v_{B-L}} \right)^2 \left[1 - \left(\frac{2M_1}{m_S} \right)^2 \right]^{1/2} \quad (2.7)$$

$$\Gamma_{N_1}^0 = \frac{\tilde{m}_1}{4\pi} \left(\frac{M_1}{v_u} \right)^2 \quad (2.8)$$

In the Froggatt-Nielsen flavor model, which serves as the basis for our previous study in Ref. [46], the masses of Higgs and (s)neutrinos, denoted as m_S , M_1 , and \tilde{m}_1 , are expected to take specific values: $m_S = 1.6 \times 10^{13} GeV$, $M_1 = 5.4 \times 10^{10} GeV$ and $\tilde{m}_1 = 4.0 \times 10^{-2} eV$. The number of free and independent parameters in this model, represented by the two neutrino masses M_1 and m_1 , correspond exactly to the two decay rates Γ_S^0 and $\Gamma_{N_1}^0$. The study was conducted in Refs. [39, 45, 46] aimed to gain a detailed and time-resolved understanding of the reheating process. A remarkable finding from this research is the presence of an approximate plateau in the radiation temperature during reheating after the B-L phase transition. This plateau occurs around the time when the heavy (s)neutrinos decay. The constancy of the temperature over an extended period is a direct result of a temporary balance between entropy production and cosmic expansion. The temperature at which this plateau occurs serves as a characteristic temperature scale for both leptogenesis and the thermal production of gravitinos. The next section will be devoted to studying the impact of B-L symmetry breaking on the gravitational wave background.

III. GRAVITATIONAL WAVES BACKGROUND

A. Primordial Gravitational Waves

Detecting the background of primordial gravitational waves would serve as compelling evidence to support the inflation paradigm, shedding light on the fundamental physics of the early Universe. In this direction, recent findings have been dedicated to studying the Primordial Gravitational Waves (PGW) at the first stages following inflation [47–54]. In the case of the inflationary scenario, the occurrence of a kinetic epoch preceding inflation results in a distinctive blue tilt in the primordial gravitational wave spectra at higher frequency ranges [55–58]. Gravitational waves are characterized as the transverse-trace-less component of the metric perturbation. In linear order perturbation theory, there is no coupling between scalar, vector, and tensor modes. Thus, for primary gravitational waves in a spatially flat FLRW background, we can express the metric element as follows:

$$ds^2 = -dt^2 + a^2(t)(\delta_{\mu\nu} + h_{\mu\nu})dx^\mu dx^\nu, \quad (3.1)$$

given that the tensor mode fulfills ($h_{\mu\mu} = h_{00} = \partial^\mu h_{\mu\mu} = 0$). $h_{\mu\nu}(t, x)$ can be decomposed into its Fourier mode, each associated with two polarization tensors which satisfy the equation of motion

$$h_{\mathbf{k}}^{\lambda\prime\prime}(\eta) + 2\mathcal{H}h_{\mathbf{k}}^{\lambda\prime}(\eta) + k^2 h_{\mathbf{k}}^\lambda(\eta) = 0, \quad (3.2)$$

where (\prime) represents the derivative with respect to conformal time η , $d\eta = \frac{dt}{a}$, and $\mathcal{H} = \frac{a'}{a}$. The normalized gravitational wave energy density spectrum is defined as the energy density per logarithmic frequency interval.

$$\Omega_{gw}(k) = \frac{1}{\rho_c} \frac{d\rho_{gw}}{d \ln k}, \quad (3.3)$$

where ρ_c is the total energy density. Moreover,

$$\Omega_{gw,0}(k) = \frac{1}{12} \left(\frac{k^2}{a_0^2 H_0^2} \right) \mathcal{P}_h(k), \quad (3.4)$$

with $\mathcal{P}_h(k) \equiv \frac{k^3}{\pi^2} \sum_\lambda |h_{\mathbf{k}}^\lambda|^2$. By considering the the scale at horizon re-entry ($k = a_{hc} H_{hc}$) and the Hubble parameter at different epochs, we can obtain the primary gravitational wave spectrum at the present time for mode re-entry during the matter (M), radiation (R), and kinetic (K) eras, respectively as follows:

$$\Omega_{gw,0}^{(M)} = \frac{1}{24} \Omega_{m,0}^2 \frac{a_0^2 H_0^2}{k^2} \mathcal{P}_t \quad (k_0 < k \leq k_{eq}), \quad (3.5)$$

$$\Omega_{gw,0}^{(R)} = \frac{1}{24} \Omega_{r,0}^2 \left(\frac{g_*}{g_{*0}} \right) \left(\frac{g_{*s}}{g_{*s0}} \right) \mathcal{P}_t \quad (k_{eq} < k \leq k_r), \quad (3.6)$$

$$\Omega_{gw,0}^{(K)} = \Omega_{gw,0}^{(R)} \left(\frac{k}{k_r} \right) \quad (k_r < k \leq k_{\max}), \quad (3.7)$$

Before we go through more details on the gravitational wave density Considering the effect of the critical value v_{B-L} and the scale k . In Fig. 3 we study the evolution of the B-L symmetry breaking parameter v_{B-L} as a function of the wavelength k considering the index spectral observational bound effects on v_{B-L} . The results are found considering the form of the tensor power spectrum from the previous section and the fact that $\mathcal{P}_t \propto k^{n_s-1}$, we conclude that considering superhorizon scales the potential parameter will decrease as we take higher values of inflation e-folds number. Additionally, the spectral index shows that for both smaller and larger scales the v_{B-L} is best considered around $2 \times 10^{15} GeV \leq v_{B-L} < 3 \times 10^{15} GeV$.

Fig. 4 represents the variation of the density of primordial gravitational waves with respect to the scale k and the v_{B-L} parameter. The color scale on the right of the plots represents the logarithm of the density of PGWs. Regions with higher color intensity (warmer colors) indicate higher density, while regions with lower color intensity (cooler colors) indicate lower density. The change in the critical value v_{B-L} that corresponds to B-L asymmetry has proportional effects on $\Omega_{gw,0}$ for all matter, radiation, and kinetic eras. In fact, as we go higher in v_{B-L} values specifically around $v_{B-L} \propto 10^{17} GeV$ we notice a significant transition in the density of PGWs. Moreover, the transition of $\Omega_{gw,0}$ corresponds to larger scales (e.g., superhorizon scales) given by $k \propto 10^6$ which are noticed only for the matter and kinetic eras. The peak region in the heat map, where the color intensity is highest, indicates the preferred combination of v_{B-L} and k that leads to the highest density of primordial gravitational waves. This combination represents the characteristic scale of the gravitational waves generated during inflation. To conclude, we

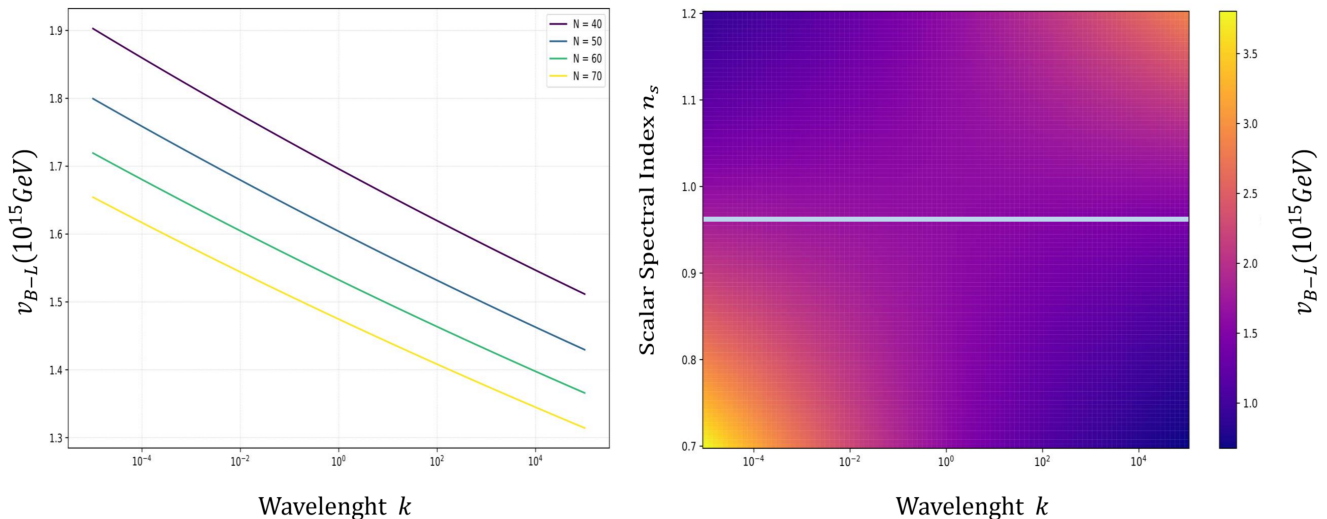


FIG. 3. The evolution of the B-L asymmetry parameter considering the variation of the scale k and the spectral index n_s .

can see that the proposed scenario of Leptogenesis has great implications for the observed values of PGWs density which can be predicted by PTA signals if made fine tuning to the values of the scale k and v_{B-L} for the matter, radiation, and kinetic eras. Next, we will see how much can the Nanograv predictions reproduce the theoretical values predicted by the chosen model of the density of PGWs.

B. Matching Gravitational Waves to the PTA Signals

The time evolution of a gravitational wave field, represented by $h_{\mathbf{k}}(\eta_i)$ at an initial conformal time η_i , and characterized by its tensor spectrum, can be obtained by determining the GW transfer function $\mathcal{T}(\eta, \mathbf{k}) = h_{\mathbf{k}}(\eta)/h_{\mathbf{k}}(\eta_i)$ [59]. Here, $h_{\mathbf{k}}(\eta)$ is evaluated at a conformal time $\eta \gg \eta_i$ [60, 61]. The relevant quantity for GW direct detection experiments, such as Pulsar Timing Arrays, are the spectral energy density parameter $\Omega_{gw}(k)$ [62]:

$$\Omega_{gw}(k) \equiv \frac{k^2}{12H_0} \mathcal{T}(\eta_0, \mathbf{k}) \mathcal{P}_t(k), \quad (3.8)$$

using η_0 to represent the present conformal time and H_0 to denote the Hubble constant [63]. For the purpose of this investigation, we focus on $\Omega_{gw}(k)$ at PTA scales, where $f \sim \mathcal{O}(10 - 9) \text{ Hz}$. The corresponding wavenumbers $k \sim \mathcal{O}(10^6) \text{ Mpc}^{-1}$ are much larger than the wavenumber associated with a mode crossing the horizon at matter-radiation equality. In other words, the modes observed on PTA scales crossed the horizon deep in the radiation era, well before the matter-radiation equality. In the regime where $k \gg k_{eq}$, the GW spectral energy density associated with PTA signals can be expressed as [64–69]:

$$\Omega_{gw}(f) = \frac{2\pi^2}{3H_0^2} A^2 \frac{f^{5-\gamma}}{f_{yr}^{\gamma-3}}. \quad (3.9)$$

The anticipated signal of the Stochastic Gravitational Wave Background (SGWB) generated by merging Black Hole Binaries (BHs) mergers corresponds to $\gamma = 13/3$ and $\alpha \simeq 5 - \gamma$. The relationship linking the amplitude of the Pulsar

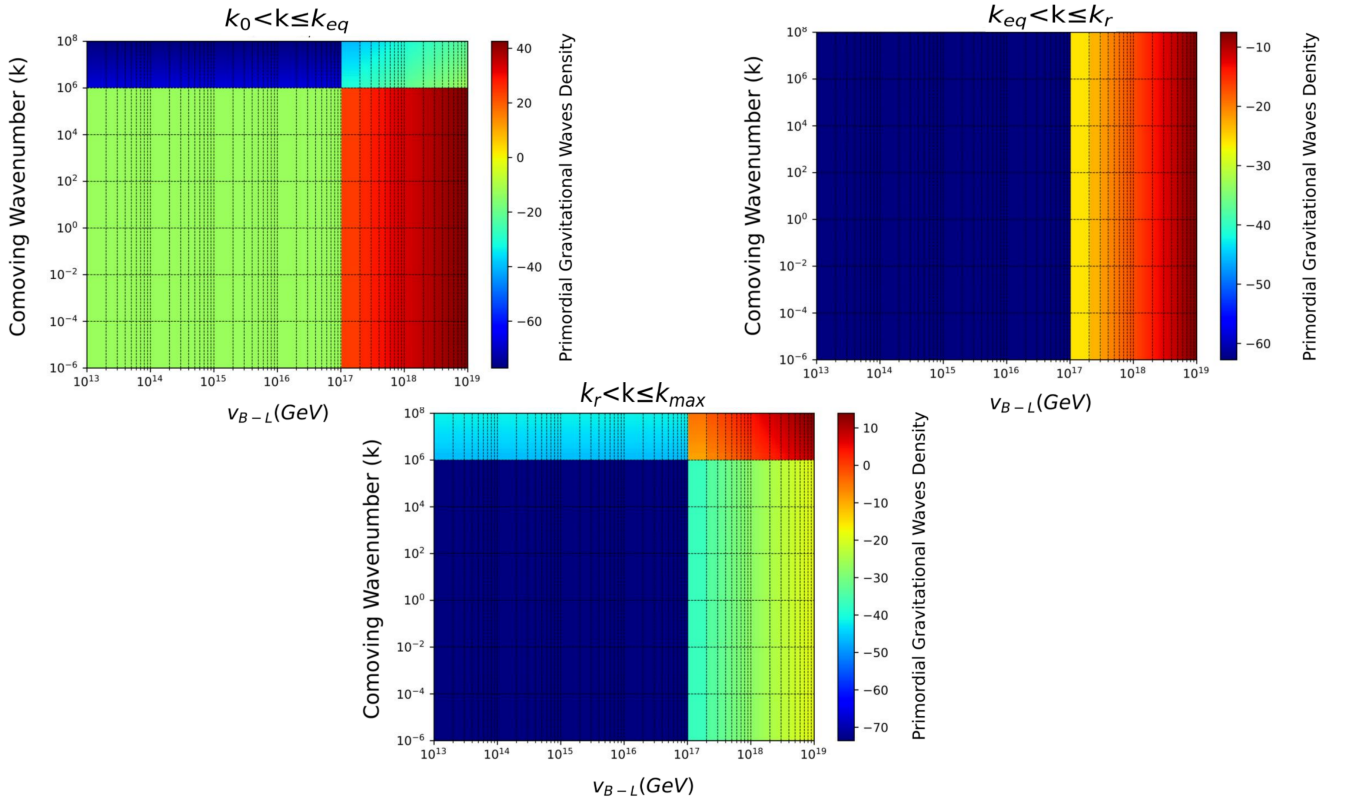


FIG. 4. Primordial gravitational wave evolution with respect to the scale k and v_{B-L} .

λ	$v_{B-L}(GeV)$	r	A	$f(Hz)$	$h^2\Omega_{gw}(f)$
1×10^{-5}	2×10^{15}	0.0174	6.02×10^{-15}	4×10^{-8}	5.06×10^{-8}
1.5×10^{-5}	2×10^{15}	0.0261	7.37×10^{-15}	2×10^{-8}	5.36×10^{-8}
2×10^{-5}	2.1×10^{15}	0.0423	9.38×10^{-15}	1×10^{-8}	6.14×10^{-8}
2×10^{-5}	2.2×10^{15}	0.0510	1.03×10^{-14}	8×10^{-7}	6.62×10^{-7}
2.5×10^{-5}	2.3×10^{15}	0.0762	1.26×10^{-14}	6×10^{-7}	8.59×10^{-7}
3×10^{-5}	2.4×10^{15}	0.1084	1.50×10^{-14}	5×10^{-7}	1.11×10^{-7}

TABLE I. Testing the density of gravitational waves predicted by PTA as functions of several parameters related to the potential considered for describing the Leptogenesis mechanism, here we've inserted the best-fit values for the cosmological parameters as per the Planck results [42], $\Omega_m = 0.315$, $\eta_0 \simeq 1.38$, $A_s = 2$, 1×10^{-9} , $k_{eq} \simeq 0.01$, $f_\star \approx 7.7 \times 10^{-17} Hz$, $f_{yr} \simeq 3.1 \times 10^{-8} Hz$ and $H_0 \equiv 100 h km/s/Mpc$.

Timing Array (PTA) signal, denoted as A , with the cosmological parameters were found to be [62, 70]

$$A = \sqrt{\frac{45\Omega_m^2 A_s}{32\pi^2(\eta_0 k_{eq})^2}} c \frac{f_{yr}}{\eta_0} \left(\frac{f_{yr}^{-1}}{f_\star} \right)^{\frac{n_T}{2}} \sqrt{r}. \quad (3.10)$$

The dependence on n_T in this context arises from the substantial "lever arm" between the Cosmic Microwave Background (CMB) pivot frequency, where A_s is constrained, and the frequency of the Pulsar Timing Array (PTA) signal [$1yr^{-1}$].

Table I corresponds to the NanoGrav proposed model of the density $h^2\Omega_{gw}(f)$ as a function of the frequency f , scalar-to-tensor ratio r , the amplitude of PTA signal that is related to the proposed potential parameters that explain the Leptogenesis phenomena. The model for $\Omega_{gw}(f)$ depends on various cosmological parameters and other constants defined previously. We compute $h^2\Omega_{gw}(f)$ is an analytical expression based on the theoretical model for primordial gravitational waves proposed recently, $h^2\Omega_{gw}(f)$ is the the fractional energy density of gravitational waves in the

universe. It represents the amount of energy carried by gravitational wave background relative to the critical energy density required to achieve a flat universe. By looking at the table identify the right parameters that can predict the higher or lower density of gravitational waves $h^2\Omega_{gw}(f)$ which reproduce the NANOGrav predictions, one can clearly see that for values of $r \lesssim 0.06$, with the spectrum is blue ($n_T > 0$) which we consider to take $n_T = 1.1$, the amplitude of PTA scales will be $A \lesssim 10^{-20}$ which will provide good predictions for $h^2\Omega_{gw}(f)$ values. Moreover, the table provides insights into the behavior of GWB density with respect to frequency, the scalar-to-tensor ratio, and the B-L asymmetry parameter, we can conclude that the results show good consistency with the predicted bounds on the density and the frequency once we fine-tune the inflationary parameter with parameters associated with the PTA signals.

IV. MATCHING PTA SIGNALS WITH GRAVITATIONAL WAVES EMITTED BY BBH MERGERS AND THE REQUIRED PBH MASS TO EXPLAIN THE JWST DATA

A. Gravitational waves from BBH mergers and PTA Interpretation

In the early universe, supermassive primordial black holes with masses around $\mathcal{O}(10^{18}M_\odot)$ could potentially emerge through various mechanisms, particularly during the radiation-dominated era. Nevertheless, before matter-radiation equality and as a consequence of the universe's expansion, multiple primordial black holes (PBHs) have the opportunity to coexist within the same Hubble patch, allowing for the formation of isolated pairs of two PBHs [71]. PBH mass can be calculated as follows [72],

$$M_{PBH} \simeq M_\odot (5 \times 10^{12} / (1 + z_f))^2 \quad (4.1)$$

In principle, binary primordial black holes (PBHs) can form either before [73], or after [74–76] matter-radiation equality. In the context of the binary black hole (BBH) merger, our focus will be on examining the observable implications of this merger rate, which is represented by a power law distribution model in the following form [77]:

$$\frac{dN_{merg}}{dt dV} \equiv \mathcal{R}(z) = R_0 (1 + z)^\alpha, \quad (4.2)$$

for a current merger rate of $R_0 = 9 - 35 \text{Gpc}^{-3} \text{yr}^{-1}$, the parameter α is determined to be $2.7_{-1.9}^{+1.8}$. The total energy released in gravitational waves, accounting for the inspiral, merging, and ringdown phases is expressed as follows [80, 81]:

$$\frac{dE_{gw}}{df} = \frac{\pi^{2/3} M_c^{5/3}}{3} \times \begin{cases} f_s^{-1/3} & \text{for } f < f_1 \\ f_1^{-1} f^{2/3} & \text{for } f_1 \leq f < f_2 \\ f_2^{-3/4} f_1^{-1} \frac{\sigma^4 f}{(\sigma^2 + 4(f - f_2)^2)^2} & \text{for } f_2 \leq f < f_3 \end{cases} \quad (4.3)$$

the GW energy spectrum of the merger, denoted as dE_{gw}/df_s , is associated with the frequency in the source frame, represented by f_s . This frequency in the source frame is related to the observed frequency, f , through the expression $f = f_{obs}(1 + z)$. The function $E(z) \equiv H(z)/H_0 = \left[\Omega_r (1 + z)^4 + \Omega_m (1 + z)^3 + \Omega_\Lambda \right]^{1/2}$, where M_c is the chirp mass, $M_c = M_{PBH}/2^{1/5}$ [71]. Analyzing the spectral attributes of the BBH background typically involves describing the energy density parameter to characterize the SGWB [82, 83]:

$$\Omega_{gw}(f)|_{f_{obs}} = \int_0^{z_{sup}} \Theta_\nu(f, z)|_{f_{obs}} \frac{d\mathcal{R}(z)}{dz} dz, \quad (4.4)$$

here $d\mathcal{R}(z)/dz$ is the expression for the differential gravitational wave event rate, while Θ_ν represents the energy flux emitted per unit frequency by a source located at a luminosity distance $d_L(z)$:

$$\Theta_\nu(f, z)|_{f_{obs}} = \frac{1}{4\pi d_L(z)^2} \frac{dE_{gw}}{df} (1 + z), \quad (4.5)$$

Ultimately, it proves beneficial to represent the model in the following form [83]

$$\begin{aligned} \Omega_{gw}(f)|_{f_{obs}} &\simeq 4.2 \times 10^{-10} \left(\frac{r_0}{3.1 \times 10^{-2} Mpc^{-3} Myr^{-1}} \right) \\ &\times \left(\frac{M_c}{8.7 M_\odot} \right)^{\frac{3}{2}} \left(\frac{f_{obs}}{100 Hz} \right)^{\frac{2}{3}}, \end{aligned} \quad (4.6)$$

As our focus is on the current energy density of gravitational waves, it becomes necessary to transform the earlier GW spectrum into a contemporary physical parameters. One can obtain the present GW spectra as functions of the observable density of GWs which can be formulated as follows:

$$\Omega_{gw,0}(f)h^2 = \Omega_{gw}(f)|_{f_{obs}} \left(\frac{g_{*j}}{g_{*0}} \right)^{-\frac{1}{3}} \Omega_{r,0}h^2 \quad (4.7)$$

here h is the present dimensionless Hubble constant and $\Omega_{r,0}h^2 \simeq 4.15 \times 10^{-5}$ is the abundance of radiation today, we choose $g_{*j}/g_{*0} = 106.75/3.36 \simeq 31$. Because gravitational waves (GWs) propagate at the speed of light, they are present in the Universe similar to radiation and add to the overall radiation energy. As a result, measurements of the total radiation density from the Cosmic Microwave Background (CMB) and Big Bang Nucleosynthesis (BBN) for species beyond the standard model can impose limitations on the overall energy density attributed to gravitational waves.

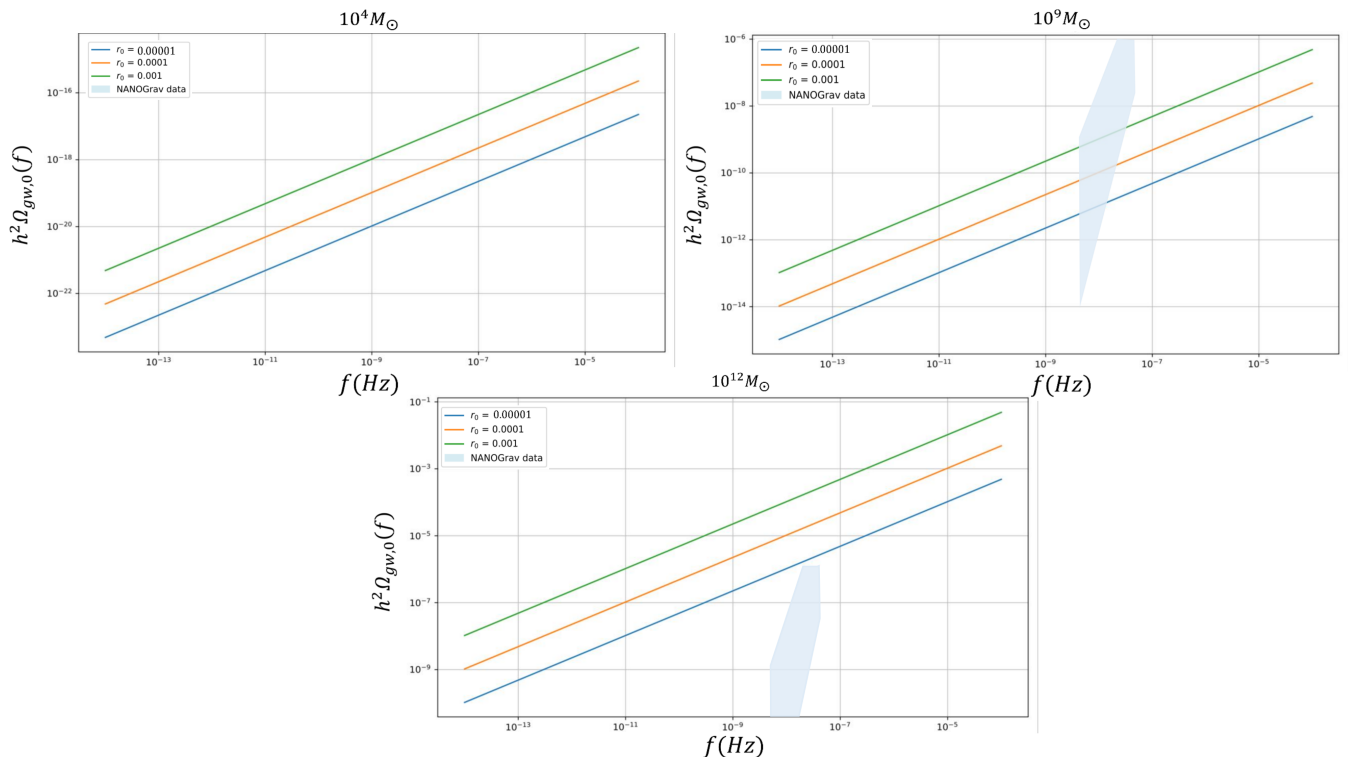


FIG. 5. Primordial gravitational waves evolution with respect to the scale and the frequency f , the light blue region represents the NANOGrav data, and r_0 is represented by three different colors for each value.

In Fig. 5, we show the abundance of the energy density of gravitational waves as a function of the present value of the frequency. We also display three expected values of $r_0 = 10^{-5}, 10^{-4},$ and 10^{-3} . We numerically compute the energy spectrum of the GWs to test the effect PBHs mass. The GW spectrum increases the frequencies and spans over the NANOGrav sensitivity region for $M_{PBH} \propto 10^9 M_\odot$. We conclude that the BBH system can partially contribute to the explanation of the energy spectrum at nanohertz frequencies. However, PBHs mass $M_{PBH} \geq 10^{12} M_\odot$ are not consistent with the expected NANOGrav GWs observatories. Moreover, the parameter r_0 of the chosen model can affect the behavior of GWs density, which means that higher values of r_0 increase the density $\Omega_{gw,0}(f)h^2$. Here, we mention that the stochastic gravitational waves from PBH binaries are important stochastic gravitational

wave background sources that are used to probe the Universe and can provide a possible explanation for the recent NANOGrav results and JWST predictions as we will see in the rest of the paper.

B. The abundance of PBH and its dependence on the B-L Breaking Mechanism

A process of PBH formation was first discussed in [84–87] which hinges on the dynamics of inflation, involving a scalar field with two distinct vacuum states. These states become unevenly distributed following the conclusion of inflation. As the universe transitions out of the inflationary phase and cools down, the expansion rate decreases. Consequently, the scalar field is allowed to move freely towards the lowest points in its potential energy. This scenario gives rise to regions within the universe where less probable vacuum states exist, surrounded by a more favored vacuum state. Essentially, this implies that once vacuum states become populated during the Friedmann–Robertson–Walker epoch, enclosed regions of less probable vacuum form, resembling islands. Over time, these closed vacuum walls can become causally connected and subsequently collapse, resulting in the formation of black holes. The mass of these black holes corresponds to that of the originating vacuum wall. Moreover, PBH formation during the early Universe generally results from the collapse of significant density fluctuations [88]. Researchers have explored limitations on the prevalence of PBHs through observations [89, 90], suggesting their abundance to be lower than 10-20 of the overall energy density of the Universe. A crucial requirement is that the density contrast needs to surpass the critical threshold of $\delta_c = 0.414$ [91]. This condition ensures the formation of PBHs during the radiation-dominated era, precisely when fluctuations come within the horizon. The estimation of primordial black hole (PBH) generation involves evaluating the portion of energy density, which is intricately linked to the variance of density perturbations. For this purpose, we employ the power spectrum alongside a window function, denoted as $W(kR)$ [92], to establish the variance $\sigma(k)$ with a final form given as [95],

$$\sigma^2 = \int_0^\infty (kR)^2 \mathcal{P}_s(k) W^2(\tilde{k}R) \frac{dk}{k}, \quad (4.8)$$

$$\sigma^2 \simeq \frac{4(1+\omega)^2}{(5+3\omega)^2} \mathcal{P}_s(k). \quad (4.9)$$

The PBH mass fraction can be obtained in an integral form when we assume the Gaussian fluctuations are given by

$$\beta \simeq \frac{1}{\sqrt{2\pi}} \frac{\sigma}{\delta_c} \exp\left(-\left(\frac{\delta_c}{\sqrt{2}\sigma}\right)^2\right). \quad (4.10)$$

The current density parameter of the PBHs can be obtained from the relation [95, 96],

$$\beta = 7.06 \times 10^{-18} \Omega_{PBH} \left(\frac{M_{PBH}}{10^{15}g}\right)^{\frac{1}{2}}.$$

Primordial black holes originate from the amplification in the initial power distribution at smaller scales. Assuming that, during a radiation-dominated phase in the Universe’s evolution, it has achieved the adiabatic limit, and the curvature perturbation on larger-than-horizon scales becomes immobilized in comoving terms. Upon the resumption of a scale entering the Hubble horizon, certain areas could exhibit a significant positive curvature, analogous to a closed Universe. During this stage, the expansion halts and a phase of contraction commences. Subsequently, the Hubble-sized area characterized by substantial positive curvature will undergo a collapse, leading to the formation of a black hole. The fraction of energy density can provide an alternative explanation for investigating the collapses of primordial black holes in the early Universe. Fig. 6 shows the fraction of the total energy density for spherically symmetric regions collapsing into PBH as a function of PBH mass for different values of v_{B-L} parameter, The results show that the curves converge toward 10^1 where the overproduction regime occurs and PBH production is satisfied, knowing that v_{B-L} has a notable effect on the behavior of the fraction of the total energy density where they converge towards values around $M_{PBH} \propto 10^{16}g$. Moreover, β shows a decreasing behavior towards higher values of the fraction β , we should note that lower values M_{PBH} results a convergence of the fraction of the total energy density towards a maximal value of β . It’s important to highlight that in this context, we’ve neglected the evolution of PBHs through processes like radiation, accretion, and merging, as these mechanisms fail to account for present-day observations. Thus, when contemplating PBH accretion as a means to form massive galaxies, we need supplementary criteria to elucidate the observations made by the JWST.

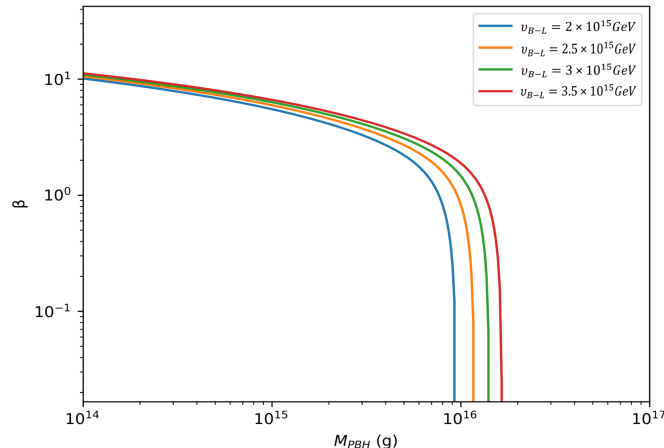


FIG. 6. The evolution of PBH mass fraction as functions of M_{PBH} for different values of the potential parameter v_{B-L} .

C. Investigating the Mass of Primordial Black Holes using JWST Observations

In recent studies, there has been significant interest in the investigation of PBHs, as they have the potential to provide insights into a range of cosmological occurrences. These include the formation of galaxies with high redshifts, the characteristics of dark matter, and the origins of supermassive black holes. After their formation, PBHs have the potential to undergo changes over cosmic time through the process of accretion. The accumulation of baryonic matter onto PBHs during this accretion phase can notably influence their mass [97, 98]. It's essential to emphasize that PBHs constitute only a small fraction of the overall dark matter content. Moreover, each PBH is enveloped by a prevailing dark matter halo, which grows over time, provided that these PBHs avoid mutual interactions [99]. Sizeable primordial black holes have the potential to act as origins of fluctuations at a specific mass scale, denoted as MB, either through the Poisson effect [100, 101] or the seed effect [102, 103]. Due to the presence of a high-density radiation field around each PBH during its formation, the fluctuation becomes stagnant in the radiation-dominated era. However, it starts to amplify during the matter-dominated era. The mass M_B , which is bound at the redshift z_B , is a key factor in this process [104].

$$M_B \approx \begin{cases} \frac{M_{PBH} f_{PBH}}{[(1+z_B) a_{eq}]^2} & (Poisson\ effect), \\ \frac{M_{PBH} f_{PBH}}{(1+z_B) a_{eq}} & (Seed\ effect), \end{cases} \quad (4.11)$$

here a_{eq} is the scale factor at the matter–radiation equality. At this point we will assume that $M_B \sim M_{halo}$ and the galaxy redshift $z \sim z_B$. Furthermore, we should introduce the star formation efficiency ε given by,

$$\varepsilon = \frac{M_*}{f_b M_{halo}}, \quad (4.12)$$

where M_{halo} is the halo mass, and f_b is the fraction of baryons in matter.

Several investigations have imposed limitations on the mass of PBHs based on the Poisson effect standpoint. Within this context, PBHs with a mass greater than $10^{11} M_\odot$ have been ruled out by multiple studies due to their non-detection, with the exception of Phoenix A [105]. Moreover, in addition to the restriction posed by the μ -distortion, PBHs with a mass around $10^5 M_\odot$ and above also face comparatively milder constraints stemming from sources such as X-ray binaries [106], PBH infall into the Galactic center influenced by dynamical friction [107], and statistical properties of the large-scale cosmic structure [104]. These combined factors necessitate that the fraction of dark matter composed of PBHs, f_{PBH} should be in the range of 10^{-4} to 10^{-3} for PBH masses spanning from around 10^5 to $10^{11} M_\odot$ [108]. Additionally, based on data from the high-redshift Lyman- α forest observations [109], primordial black holes with $M_{PBH} f_{PBH} \gtrsim 170 M_\odot$ and $f_{PBH} > 0.05$ have been excluded. This indicates a significant unfavorable stance towards the existence of supermassive PBHs capable of contributing to the Poisson effect. In Fig.

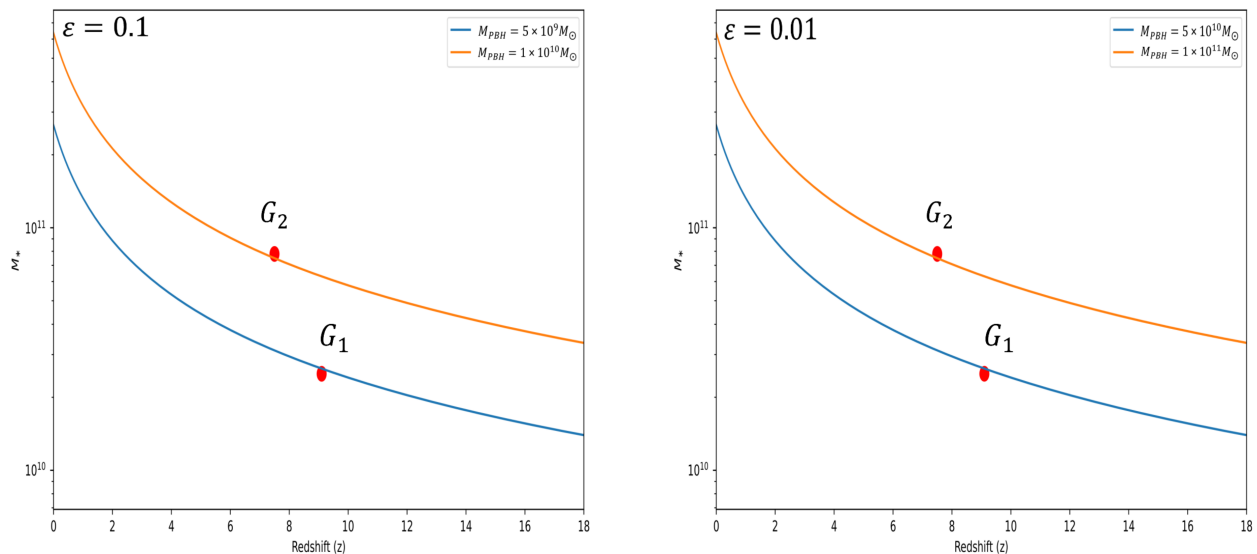


FIG. 7. The evolution of galaxies stellar masses M_* as a function of the redshift for different values of the PBH mass M_{PBH} , the two dots represent the two most massive high- z objects, galaxies 35300 and 38094 referred as G_1 and G_2 respectively.

7 we have plotted the variation of galaxies' stellar masses M_* as functions of the redshift z , we observe that the stellar mass decreases slowly with respect to the redshift towards stable values. Moreover, the galaxy formation efficiency ε has a notable effect on the PBH mass M_{PBH} which could get lower as we take higher values of ε . Finally, the influence of the seed effect, which operates on smaller scales, remains a viable explanation for interpreting the observations made by the JWST observation.

V. ASSESSMENT OF JWST OBSERVATIONS: VERIFYING RAPID ACCRETION RATES OF PBHS

Recent studies indicate that the farthest quasars identified to date, with redshifts around $[6, 7.5]$, are fueled by supermassive black holes (SMBHs) weighing approximately $10^8 M_\odot$ to $10^{10} M_\odot$ [110–116]. The presence of these immense black holes poses a challenge to current theoretical models of black hole formation and evolution, as critical details such as the nature and mass of the SMBH seeds, as well as their ability to grow rapidly enough to reach SMBH status within the first billion years of the Universe, remain unresolved. Investigating supermassive black holes of around $10^6 M_\odot$ to $10^7 M_\odot$ solar masses at redshifts $z > 9$ is crucial for advancing our understanding in this field [117, 118]. The recent assertion of a highly active supermassive black hole in GN-z11, a renowned galaxy undergoing star formation at $z = 10.6$ [119] aligns with this pursuit. GN-z11 was initially detected by [120, 121] and subsequently examined in the JWST Advanced Deep Extragalactic Survey [122] using NIRSpec spectroscopy [123] and NIRCам imaging [124]. These observations indicate that GN-z11 exhibits characteristics consistent with an Active Galactic Nucleus (AGN), supported by several pieces of evidence namely the presence of high ionization transitions [125]. Moreover, commonly associated with AGNs, as they necessitate high photon energies typically not generated by stars [126, 127].

It's generally assumed that Nuclear Black Holes (BHs) enlarge by drawing in gas from the nearby environment. This accretion process is governed by both star formation and mechanical feedback mechanisms, both of which result in a reduction of gas within the galaxy hosting the BH. According to [128–130], it's postulated that nuclear BHs

accrete gas according to the Bondi-Hoyle-Lyttleton (BHL) accretion rate formula:

$$\dot{M}_{blondi} = \frac{4\pi G^2 M_{BH}^2 \langle \rho_{gas} \rangle}{\left(\langle c_s \rangle^2 + \langle \nu_{BH} \rangle^2 \right)^{3/2}}, \quad (5.1)$$

In the above equation c_s is the sound speed, ν_{BH} is the velocity of the BH relative to the gas, M_{BH} is the mass of the BH , ρ_{gas} is the gas density, G is the gravitational constant. The accretion rate of the black hole is limited to the Eddington value. A portion, represented by $\varepsilon \dot{M}_{accr}$, of the mass being accreted is transformed into radiation. Therefore, the effective rate of growth of the black hole's mass can be expressed as $\dot{M}_{BH} = (1 - \varepsilon) \dot{M}_{accr}$.

In the following, we will apply the accretion laws in the context of PBHs that we assume as seeds for the observed AGNs. Similarly to [131], we suggest that the bolometric luminosity, denoted as

$$L_{bol} = \varepsilon \dot{M}_{PBH} c^2, \quad (5.2)$$

is evenly distributed thermally and isotropically among the gas particles within the smoothing volume surrounding the PBH. The Eddington ratio [132], denoted as $\Gamma = L_{bol}/L_{Edd}$, represents the relationship between the bolometric luminosity of a quasar and its Eddington luminosity. This ratio is formulated under the assumption of hydrostatic equilibrium and pure ionized hydrogen and can be expressed as:

$$L_{Edd} = \frac{4\pi M_{PBH} m_p c}{\sigma_T}, \quad (5.3)$$

here m_p is the mass of a proton and σ_T is the Thomson scattering cross-section. In this research, we proposed that the BHL accretion model offers a potential explanation, wherein PBHs accrete surrounding gas from the interstellar medium at a rate dependent on their mass, relative velocity, and local gas density. This model, combined with the Eddington limit which sets an upper bound on the luminosity and thus the accretion rate based on the balance between radiation pressure and gravitational pull can describe the rapid growth phases of these black holes. If PBHs can accrete at near-Eddington or even super-Eddington rates under certain conditions, such as dense gas environments or during periods of high gas inflow, it would help explain how these distant SMBHs accumulated mass so quickly. By applying the Eddington accretion rate and the bolometric luminosity which are directly proportional to the efficiency factor ε and PBH mass, we can better understand the dynamics and efficiency of early black hole growth, potentially resolving the puzzle of their rapid formation and contributing to our knowledge of the early universe's evolution.

Fig. 8 shows the mass accretion rate onto PBHs as a function of the Eddington ratio Γ across different redshifts z , reflecting various epochs in the early universe. The results are plotted on a logarithmic scale. The left side of the plot shows the relationship between the Eddington ratio and the accretion rate, with shaded regions, the red one highlights values below the Eddington limit and the blue region represents values above the Eddington limit, the results are plotted for different values of the redshift $z \sim [4, 12]$, we noticed that the accretion rate of PBHs as a function of the ratio Γ is only noticeable around $\dot{M}_{PBH} \propto 10^{29} kg/s$. Moreover, increasing the redshift values makes the accretion rate faster when crossing the Eddington limit $\Gamma \sim 1$. On the right side, The accretion rate is computed for a range of Eddington ratios and redshifts, forming a two-dimensional grid of values. The results are displayed in a contour plot, showing the logarithm of the mass accretion rate across different redshifts and Eddington ratios. An Eddington limit line is included to indicate the boundary between sub-Eddington and super-Eddington accretion. Additionally, colored regions highlight specific redshift bounds where early galaxies and quasars have been observed by the JWST. Following these results we conclude that the accretion of PBHs can be considered as sub-Eddington when we consider values below $\dot{M}_{PBH} \lesssim 10^{28} kg/s$ for the lower bound on the redshift that corresponds to quasars observations and the higher bound related to early Galaxies observations, while both redshift regions are considered super-Eddington for $\dot{M}_{PBH} \gtrsim 10^{28} kg/s$.

Fig. 9 visualizes galaxies' stellar masses required to achieve certain Eddington luminosities across various redshifts. The results are presented in a contour plot, showing the logarithm of the stellar mass as a function of logarithmic Eddington luminosity and redshift, with additional vertical lines indicating specific limits of Eddington luminosity values of PBHs of different masses. Shaded regions highlight redshift bounds corresponding to observations of quasars and early galaxies by the JWST. For both cases of the redshift bounds, we found that the Eddington limit can increase when taking higher values of PBHs masses. In fact, this model can provide a much clearer idea on the sub- or super-Eddington luminosity of stellar masses taking into account the redshift values and PBHs masses, we conclude that for the lowest chosen PBH masse $M_{PBH} \propto 10^6 M_\odot$ the Eddington limit can reach $L_{Edd} \sim 10^{38.5} W \sim 10^{11} L_\odot$, while for the highest chosen PBH masse $M_{PBH} \propto 10^{10} M_\odot$ the Eddington limit became $L_{Edd} \sim 10^{42.5} W \sim 10^{15} L_\odot$. This visualization helps in understanding the conditions under which PBHs could grow rapidly, potentially explaining the formation of the most distant and massive black holes observed, and providing insights into the accretion dynamics and the role of PBHs in cosmic evolution.

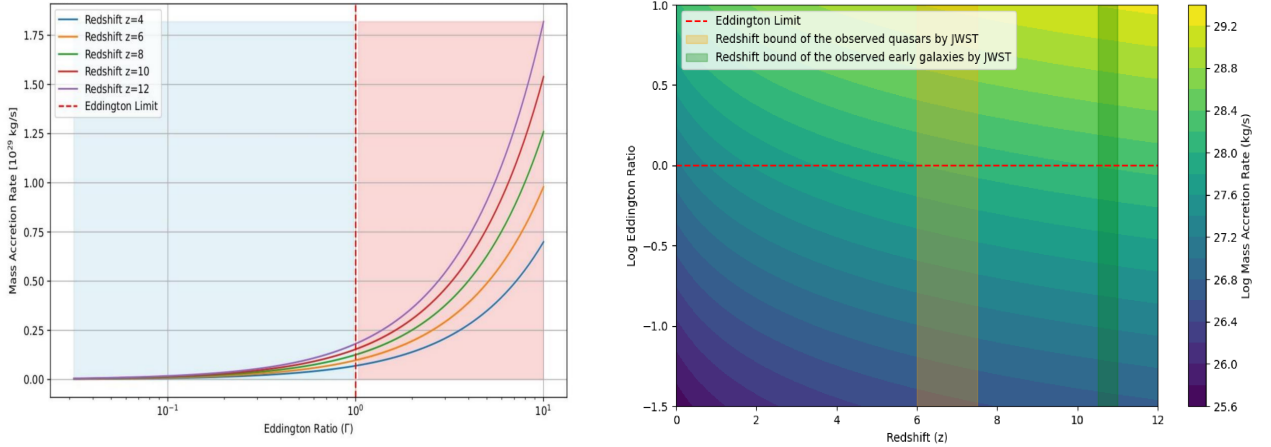


FIG. 8. The mass accretion rate of primordial black holes as a function of the Eddington ratio for different redshifts.

Fig. 10 investigates the relationship between the mass of PBHs, their Eddington ratios, and redshifts. The results are displayed in a contour plot, showcasing the logarithm of PBH masses across different Eddington ratios and redshifts. This visualization offers insights into the growth potential of PBHs in the early universe and how their masses vary with changing accretion rates and cosmic epochs. Additionally, shaded regions highlight redshift bounds corresponding to observations of early galaxies and quasars by the JWST, emphasizing the relevance of the study to current observational constraints. The Eddington limit line shows the boundary between sub-Eddington and super-Eddington regimes, providing context for the efficiency of PBH accretion. Furthermore, the blue dots represent the observed quasars powered by SMBHs based on recent observations. It also includes red dots which symbolize observations of GN-z11 AGN, suggesting these might be powered by MPBHs. Finally, the purple dots denote extreme cases of PBHs with masses between $10^8 M_\odot$ and $10^{10} M_\odot$. From these results we conclude that the choice of the accretion rate plays an essential role in understanding galaxy formation and black hole growth from different eras in our Universe, we can also see that lower PBHs accretion speed of around $\propto 10^6 \text{ kg/s}$ can enable the existence of the estimated MBHs of AGNs like GN-z11 on sub-Eddington rate for masses $M_{PBH} \lesssim 10^6 M_\odot$, and super-Eddington for higher masses. Moreover, the higher the accretion rate became the earlier MBHs and SMBHs can exist either in the early Universe or subsequent eras. In fact, an accretion speed around $\propto 10^8 \text{ kg/s}$ can make the process of MBH's AGNs on sub-Eddington regime, and SMBHs formation possible with super-Eddington rate for masses $M_{PBH} \gtrsim 10^7 M_\odot$, while for accretion speed $M_{PBH} \propto 10^{12} \text{ kg/s}$, it is possible to have SMBHs that powers the observed quasars around $z \sim 6 - 7$ with sub-Eddington rate for masses $M_{PBH} \lesssim 10^9 M_\odot$ and super-Eddington rate for higher masses, while extreme cases of PBHs masses can co-exist on the same rate of accretion condition and masse constraints. Overall, this program contributes to understanding the formation and evolution of PBHs in the early universe, offering valuable insights into their role in cosmic structure formation and the growth of supermassive black holes.

VI. CONCLUSION

The process of B-L symmetry breaking at the Grand Unified Theory scale can be counted as an additional factor for the initial conditions of the Universe, which affects the entropy, the occurrence of baryogenesis through leptogenesis, and the formation of dark matter due to the thermal generation of gravitinos. In the preceding sections, we computed

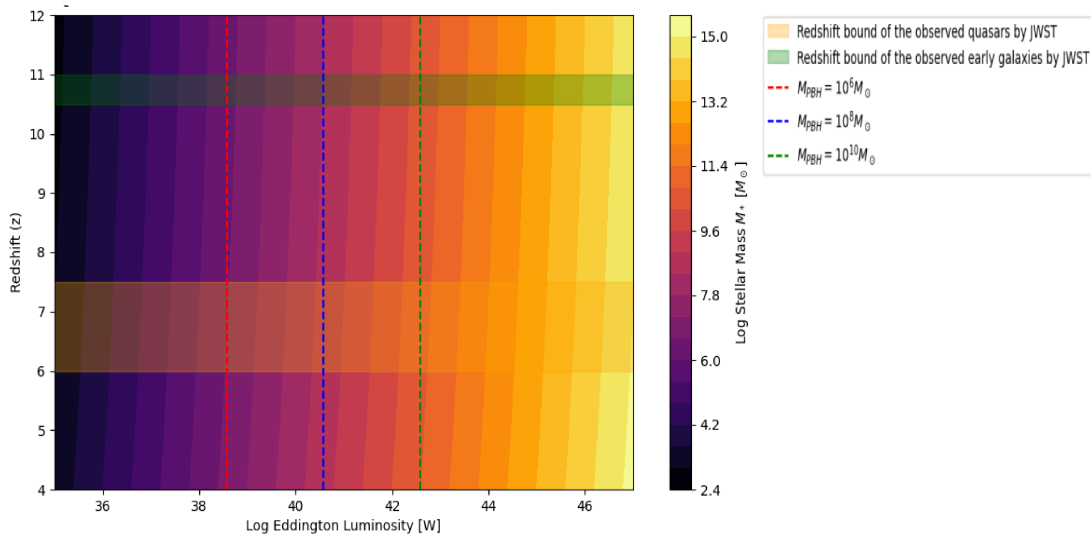


FIG. 9. Stellar Mass as a Function of Logarithmic Eddington Luminosity and Redshift Across Different Cosmic Epochs.

the gravitational wave pattern resulting from the cosmological breaking of B-L symmetry. This process occurred due to several factors, including the era of inflation, the phase transition of the Universe, Cosmic strings, and the gravitational waves linked to binary systems of black holes forming in the early Universe. Additionally, our focus was directed toward the JWST predictions related to the PBH masses and the early galaxy formation.

To go into further detail, our findings show first that considering the scalar potential governing the B-L symmetry breaking mechanism, the model parameter λ shows good consistency for a wide range of model parameters with the latest observations from Planck data. As for the critical value of the phase transition parameter v_{B-L} , the results show that it must be bounded around $\sim [2 \times 10^{15}, 5 \times 10^{15}] GeV$, our findings also align with earlier findings that suggested tuning the v_{B-L} value to be close to the GUT scale. Moreover, when we study the evolution of the B-L symmetry breaking parameter v_{B-L} as a function of the wavelength k , we conclude that considering superhorizon scales the potential parameter will decrease as we take higher values of inflation e-fold number. Additionally, the spectral index shows that for both smaller and larger scales the v_{B-L} is best considered around the previously observed values. On the other hand, for the variation of the density of primordial gravitational waves with respect to the scale k and v_{B-L} for different phases, we found that the change in the critical value v_{B-L} that corresponds to B-L asymmetry has a proportional effect on $\Omega_{gw,0}(f)$ for all matter, radiation, and kinetic eras, from the results, we see that the proposed scenario of Leptogenesis has great implications of the observed values of PGWs density which can be predicted by PTA signals.

Moreover, we studied the NanoGrav proposed model of the density $h^2\Omega_{gw}(f)$ as a function of the frequency f , scalar-to-tensor ratio r , and the amplitude of the PTA signal that relates to the proposed potential parameters that explain the Leptogenesis phenomena, we identified the right parameters that can predict higher or lower density of gravitational waves that reproduced the NANOGrav predictions, the results show good consistency with the predicted bounds on the density and the frequency once we fine-tune the inflationary parameter with parameters associated with the PTA signals.

We have calculated the density of gravitational waves from BBH mergers that can be predicted by PTA interpretation, we conclude that the BBH system can partially contribute to the explanation of the energy spectrum at nanohertz frequencies. Moreover, PBH mass around $M_{PBH} \propto 10^9 M_\odot$ presents the best fit with recent NANOGrav data. Additionally, PBH binaries are important stochastic gravitational wave background sources that are used to probe the Universe and can provide a possible explanation for the recent NANOGrav results and JWST predictions. On another hand, when we study PBH formation v_{B-L} has a notable effect on the behavior of the fraction of the total energy density where they converge towards values $M_{PBH} \propto 10^{16} g$. However, the mass of PBH at the formation time fail to explain recent data, for this reason, we need to consider that the evolution of PBHs has already happened which leads to massive galaxies formation, then supplementary criteria will be considered to explain the observations made by the JWST. The variation of galaxies stellar masses M_* as functions of the redshift z , has shown that the

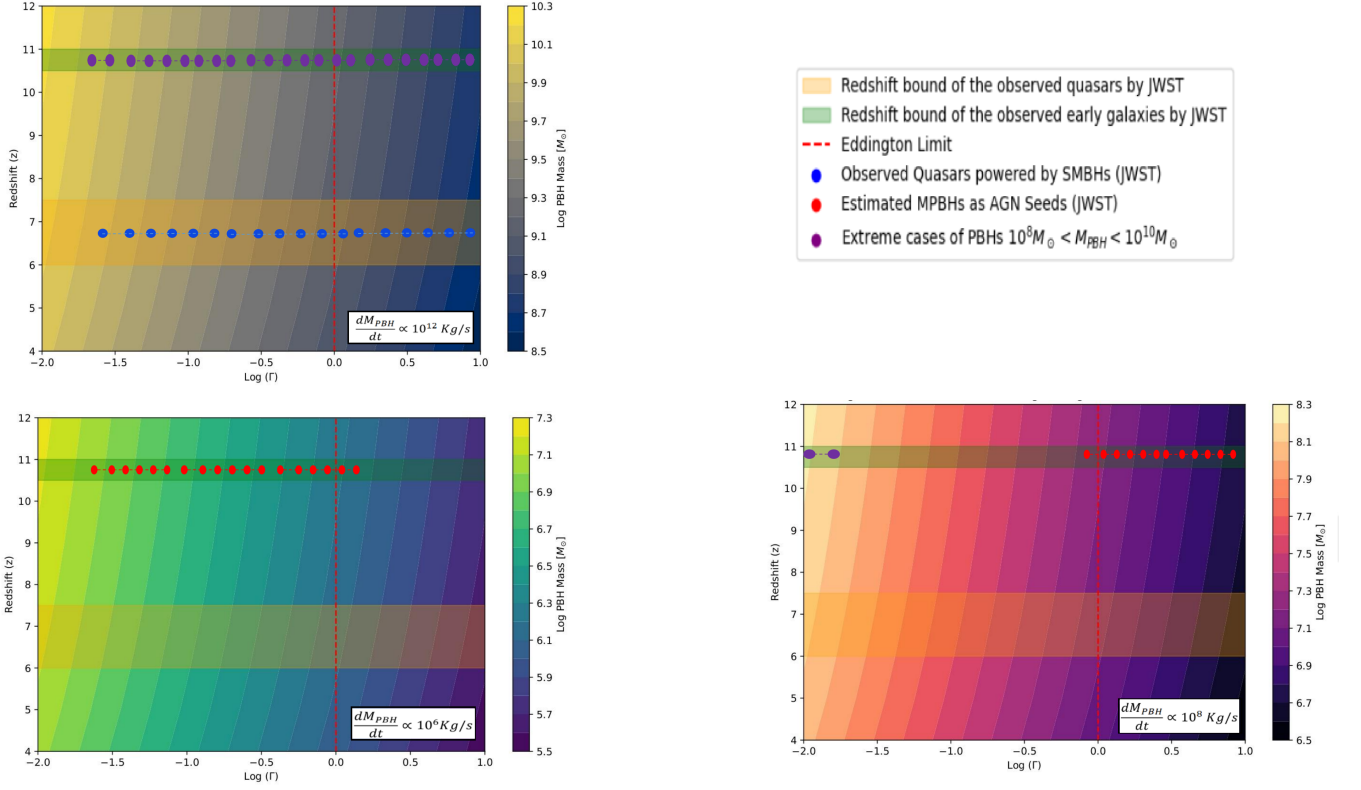


FIG. 10. Primordial Black Hole Mass Across Eddington Ratios and Redshifts.

galaxy formation efficiency has a notable effect on the PBH mass, then the influence of the seed, effect remains a viable tool for interpreting the JWST observations.

In our study, we apply the Bondi-Hoyle-Lyttleton (BHL) accretion model to primordial black holes (PBHs) as seeds for the observed AGNs, suggesting that PBHs can accrete surrounding gas at rates dependent on their mass, relative velocity, and local gas density. This model, combined with the Eddington limit which balances radiation pressure against gravitational pull can describe the rapid growth phases of these black holes. Our results indicate that PBHs can accrete at near-Eddington or super-Eddington rates under specific conditions, such as dense gas environments or periods of high gas inflow, potentially explaining the rapid mass accumulation of these distant SMBHs. We conclude that the BHL accretion model, when integrated with the Eddington accretion rate and bolometric luminosity proportional to the efficiency factor ε and PBH mass, provides insights into the dynamics and efficiency of early black hole growth. This could help resolve the puzzle of their rapid formation and enhance our understanding of the early Universe's evolution.

ACKNOWLEDGEMENTS

The work by M.K. was performed with the financial support provided by the Russian Ministry of Science and Higher Education, project “Fundamental and applied research of cosmic rays”, No. FSWU-2023-0068..

-
- [1] Starobinsky, Alexei A. *Relict gravitation radiation spectrum and initial state of the universe*. JETP lett 30.682-685 (1979): 131-132.
 - [2] Rubakov, V. A., Sazhin, M. V., & Veryaskin, A. V. (1982). *Graviton creation in the inflationary universe and the grand unification scale*. Physics Letters B, 115(3), 189-192.
 - [3] Blasi, S., Brdar, V., & Schmitz, K. (2021). Has NANOGrav found first evidence for cosmic strings?. Physical Review Letters, 126(4), 041305.

- [4] Ellis, J., & Lewicki, M. (2021). *Cosmic string interpretation of NANOGrav pulsar timing data*. Physical Review Letters, 126(4), 041304.
- [5] Mandic, V., Bird, S., & Cholis, I. (2016). *Stochastic gravitational-wave background due to primordial binary black hole mergers*. Physical review letters, 117(20), 201102.
- [6] Fukugita, M., & Yanagida, T. (1986). *Barygenesis without grand unification*. Physics Letters B, 174(1), 45-47.
- [7] Lazarides, G., & Shafi, Q. (1991). *Origin of matter in the inflationary cosmology*. Physics Letters B, 258(3-4), 305-309.
- [8] Yanagida, T. (1979). Proc. *Workshop on Unified theory and the baryon number in the universe*. KEK Report No. 79-18, 95.
- [9] Gell-Mann, M., Ramond, P., & Slansky, R. (1979). *Supergravity ed P van Nieuwenhuizen and DZ Freedman*. Amsterdam: North-Holland) p, 315, 79-18.
- [10] Fukugita, M., & Yanagida, T. (1986). *Barygenesis without grand unification*. Physics Letters B, 174(1), 45-47.
- [11] Buchmüller, W., & Plümacher, M. (1999). *Matter-antimatter asymmetry and neutrino properties*. Physics reports, 320(1-6), 329-339.
- [12] Faessler, A., Kosmas, T. S., Leontaris, G. K., & Lazarides, G. (2000). *Leptogenesis in supersymmetric hybrid inflation*. Symmetries in intermediate and high energy physics, 227-245.
- [13] Asaka, T., Hamaguchi, K., Kawasaki, M., & Yanagida, T. (1999). *Leptogenesis in inflaton decay*. Physics Letters B, 464(1-2), 12-18.
- [14] Campbell, B. A., Davidson, S., & Olive, K. A. (1993). *Inflation, neutrino baryogenesis, and (s) neutrino-induced baryogenesis*. Nuclear Physics B, 399(1), 111-136.
- [15] Khlopov, M. Y., & Linde, A. D. (1984). *Is it easy to save the gravitino?*. Physics Letters B, 138(4), 265-268.
- [16] Ellis, J., Kim, J. E., & Nanopoulos, D. V. (1984). *Cosmological gravitino regeneration and decay*. Physics Letters B, 145(3-4), 181-186.
- [17] Bolz, M., Buchmüller, W., & Plümacher, M. (1998). *Baryon asymmetry and dark matter*. Physics Letters B, 443(1-4), 209-213.
- [18] Khlopov, M. Y., Levitan, Y. L., Sedel’Nikov, E. V., & Sobol, I. M. (1994). *Nonequilibrium cosmological nucleosynthesis of light elements: Calculations by the Monte Carlo method*. Physics of Atomic Nuclei, 57(8), 1393-1397.
- [19] Khlopov, M. Y., Barrau, A., & Grain, J. (2006). *Gravitino production by primordial black hole evaporation and constraints on the inhomogeneity of the early universe*. Classical and Quantum Gravity, 23(6), 1875.
- [20] Balestra, F. (1984). *Annihilation of antiprotons with Helium-4 at low energies and its relationship with the problems of the modern cosmology and models of grand unification*. Sov. J. Nucl. Phys, 39, 626-631.
- [21] Antoniadis, J., Arumugam, P., Arumugam, S., Babak, S., Bagchi, M., Nielsen, A. S. B., ... & Wu, Z. (2023). *The second data release from the European Pulsar Timing Array III. Search for gravitational wave signals*. arXiv preprint arXiv:2306.16214.
- [22] Antoniadis, J., Arumugam, P., Arumugam, S., Babak, S., Bagchi, M., Nielsen, A. S. B., ... & Wu, Z. (2023). *The second data release from the European Pulsar Timing Array. Implications for massive black holes, dark matter and the early Universe*, 2306.
- [23] Zic, A., Reardon, D. J., Kapur, A., Hobbs, G., Mandow, R., Curylo, M., ... & Zhu, X. J. (2023). *The Parkes Pulsar Timing Array Third Data Release*. Publications of the Astronomical Society of Australia, 1-15.
- [24] Rubin, S. G., Sakharov, A. S., & Khlopov, M. Y. (2001). *The formation of primary galactic nuclei during phase transitions in the early universe*. Journal of Experimental and Theoretical Physics, 92, 921-929.
- [25] Belotsky, K. M., Dokuchaev, V. I., Eroshenko, Y. N., Esipova, E. A., Khlopov, M. Y., Khromykh, L. A., ... & Svadkovsky, I. V. (2019). *Clusters of primordial black holes*. The European Physical Journal C, 79, 1-20.
- [26] Naidu, R. P., Oesch, P. A., van Dokkum, P., Nelson, E. J., Suess, K. A., Brammer, G., ... & Weibel, A. (2022). *Two remarkably luminous galaxy candidates at $z \approx 10 - 12$ revealed by JWST*. The Astrophysical Journal Letters, 940(1), L14.
- [27] Adams, N. J., Conselice, C. J., Ferreira, L., Austin, D., Trussler, J. A. A., Juodžbalis, I., ... & Vijayan, A. P. (2023). *Discovery and properties of ultra-high redshift galaxies ($9 < z < 12$) in the JWST ERO SMACS 0723 Field*. Monthly Notices of the Royal Astronomical Society, 518(3), 4755-4766.
- [28] Yan, H., Ma, Z., Ling, C., Cheng, C., & Huang, J. S. (2022). *First batch of candidate galaxies at redshifts 11 to 20 revealed by the James Webb Space Telescope early release observations*. arXiv preprint arXiv:2207.11558.
- [29] Labbe, I., van Dokkum, P., Nelson, E., Bezanson, R., Suess, K., Leja, J., ... & Stefanon, M. (2022). *A very early onset of massive galaxy formation*. arXiv preprint arXiv:2207.12446.
- [30] Y.B. Zel’dovich and I.D. Novikov, *The Hypothesis of Cores Retarded during Expansion and the Hot Cosmological Model*, Soviet Astron. AJ (Engl. Transl.), 10 (1967) 602.
- [31] Hawking, S. (1971). *Gravitationally collapsed objects of very low mass*. Monthly Notices of the Royal Astronomical Society, 152(1), 75-78.
- [32] Bavera, S. S., Franciolini, G., Cusin, G., Riotto, A., Zevin, M., & Fragos, T. (2022). *Stochastic gravitational-wave background as a tool for investigating multi-channel astrophysical and primordial black-hole mergers*. Astronomy & Astrophysics, 660, A26.
- [33] Abbott, R., Abbott, T. D., Acernese, F., Ackley, K., Adams, C., Adhikari, N., ... & Brinkmann, M. (2022). *Search for Subsolar-Mass Binaries in the First Half of Advanced LIGO’s and Advanced Virgo’s Third Observing Run*. Physical review letters, 129(6), 061104.
- [34] Carr, B., & Kühnel, F. (2020). *Primordial black holes as dark matter: recent developments*. Annual Review of Nuclear and Particle Science, 70, 355-394.

- [35] Hoyle, F., & Narlikar, J. V. (1966). *On the formation of elliptical galaxies*. Proceedings of the Royal Society of London. Series A. Mathematical and Physical Sciences, 290(1421), 177-185.
- [36] Carr, B. J., & Silk, J. (1983). *Can graininess in the early universe make galaxies?*. Astrophysical Journal, Part 1 (ISSN 0004-637X), vol. 268, May 1, 1983, p. 1-16., 268, 1-16.
- [37] Carr, B. J., & Rees, M. J. (1984). *Can pregalactic objects generate galaxies?*. Monthly Notices of the Royal Astronomical Society, 206(4), 801-818.
- [38] Datta, S. (2023). *Inflationary gravitational waves, pulsar timing data and low-scale-leptogenesis*. arXiv preprint arXiv:2307.00646.
- [39] Buchmüller, W., Domcke, V., Kamada, K., & Schmitz, K. (2013). *The gravitational wave spectrum from cosmological B-L breaking*. Journal of Cosmology and Astroparticle Physics, 2013(10), 003.
- [40] Gell-Mann, M., Ramond, P., & Slansky, R. (1979). *Supergravity ed P van Nieuwenhuizen and DZ Freedman*. Amsterdam: North-Holland p, 315, 79-18.
- [41] Yanagida, T. (1979). *Proc. Workshop on Unified theory and the baryon number in the universe*. KEK Report No. 79-18, 95.
- [42] Aghanim, N., Akrami, Y., Ashdown, M., Aumont, J., Baccigalupi, C., Ballardini, M., ... & Roudier, G. (2020). *Planck 2018 results-VI. Cosmological parameters*. Astronomy & Astrophysics, 641, A6.
- [43] Baumann, D. (2009). *TASI lectures on inflation*. arXiv preprint arXiv:0907.5424.
- [44] Nakayama, K., Takahashi, F., & Yanagida, T. T. (2010). *Constraint on the gravitino mass in hybrid inflation*. Journal of Cosmology and Astroparticle Physics, 2010(12), 010.
- [45] Buchmüller, W., Domcke, V., & Schmitz, K. (2012). *Spontaneous B-L breaking as the origin of the hot early universe*. Nuclear Physics B, 862(3), 587-632.
- [46] Sahu, N., & Yajnik, U. A. (2005). *Gauged B-L symmetry and baryogenesis via leptogenesis at TeV scale*. Physical Review D, 71(2), 023507.
- [47] El Bourakadi, K., Ferricha-Alami, M., Filali, H., Sakhi, Z., & Bennai, M. (2021). *Gravitational waves from preheating in Gauss-Bonnet inflation*. The European Physical Journal C, 81(12), 1144.
- [48] El Bourakadi, K., Asfour, B., Sakhi, Z., Bennai, M., & Ouali, T. (2022). *Primordial black holes and gravitational waves in teleparallel Gravity*. The European Physical Journal C, 82(9), 792.
- [49] El Bourakadi, K., Bousder, M., Sakhi, Z., & Bennai, M. (2021). *Preheating and reheating constraints in supersymmetric braneworld inflation*. The European Physical Journal Plus, 136(8), 1-19.
- [50] Sakhi, Z., El Bourakadi, K., Safsafi, A., Ferricha-Alami, M., Chakir, H., & Bennai, M. (2020). *Effect of brane tension on reheating parameters in small field inflation according to Planck-2018 data*. International Journal of Modern Physics A, 35(30), 2050191.
- [51] Bousder, M., El Bourakadi, K., & Bennai, M. (2021). *Charged 4d einstein-gauss-bonnet black hole: Vacuum solutions, cauchy horizon, thermodynamics*. Physics of the Dark Universe, 32, 100839.
- [52] El Bourakadi, K., Sakhi, Z., & Bennai, M. (2022). *Preheating constraints in α -attractor inflation and Gravitational Waves production*. International Journal of Modern Physics A, 37(17), 2250117.
- [53] El Bourakadi, K., Koussour, M., Otalora, G., Bennai, M., & Ouali, T. (2023). *Constant-roll and primordial black holes in $f(Q, T)$ gravity*. Physics of the Dark Universe, 41, 101246.
- [54] Bourakadi, K. E., Ferricha-Alami, M., Sakhi, Z., Bennai, M., & Chakir, H. (2023). *Dark matter via Baryogenesis: Affleck-Dine Mechanism in the Minimal Supersymmetric Standard Model*. arXiv preprint arXiv:2307.15541.
- [55] Sahni, V., Sami, M., & Souradeep, T. (2001). *Relic gravity waves from braneworld inflation*. Physical Review D, 65(2), 023518.
- [56] Figueroa, D. G., & Tanin, E. H. (2019). *Inconsistency of an inflationary sector coupled only to Einstein gravity*. Journal of Cosmology and Astroparticle Physics, 2019(10), 050.
- [57] Giovannini, M. (1998). *Gravitational wave constraints on post-inflationary phases stiffer than radiation*. Physical Review D, 58(8), 083504.
- [58] Riazuelo, A., & Uzan, J. P. (2000). *Quintessence and gravitational waves*. Physical Review D, 62(8), 083506.
- [59] Baumann, D., Steinhardt, P., Takahashi, K., & Ichiki, K. (2007). *Gravitational wave spectrum induced by primordial scalar perturbations*. Physical Review D, 76(8), 084019.
- [60] Vagnozzi, S. (2021). *Implications of the NANOGrav results for inflation*. Monthly Notices of the Royal Astronomical Society: Letters, 502(1), L11-L15.
- [61] Zhao, W., Zhang, Y., You, X. P., & Zhu, Z. H. (2013). *Constraints of relic gravitational waves by pulsar timing arrays: Forecasts for the FAST and SKA projects*. Physical Review D, 87(12), 124012.
- [62] Vagnozzi, S. (2023). *Inflationary interpretation of the stochastic gravitational wave background signal detected by pulsar timing array experiments*. Journal of High Energy Astrophysics.
- [63] Kuroyanagi, S., Chiba, T., & Sugiyama, N. (2009). *Precision calculations of the gravitational wave background spectrum from inflation*. Physical Review D, 79(10), 103501.
- [64] Afzal, A., Agazie, G., Anumarlapudi, A., Archibald, A. M., Arzoumanian, Z., Baker, P. T., ... & NANOGrav Collaboration. (2023). *The NANOGrav 15 yr Data Set: Search for Signals from New Physics*. The Astrophysical Journal Letters, 951(1), L11.
- [65] Agazie, G., Anumarlapudi, A., Archibald, A. M., Arzoumanian, Z., Baker, P. T., Bécsy, B., ... & NANOGrav Collaboration. (2023). *The NANOGrav 15 yr data set: Evidence for a gravitational-wave background*. The Astrophysical Journal Letters, 951(1), L8.

- [66] Agazie, G., Alam, M. F., Anumalapudi, A., Archibald, A. M., Arzoumanian, Z., Baker, P. T., ... & NANOGrav Collaboration. (2023). *The NANOGrav 15 yr Data Set: Observations and Timing of 68 Millisecond Pulsars*. The Astrophysical Journal Letters, 951(1), L9.
- [67] Arzoumanian, Z., Baker, P. T., Blumer, H., Bécsy, B., Brazier, A., Brook, P. R., ... & NANOGrav Collaboration. (2020). *The NANOGrav 12.5 yr data set: search for an isotropic stochastic gravitational-wave background*. The Astrophysical Journal Letters, 905(2), L34.
- [68] Arzoumanian, Z., Brazier, A., Burke-Spolaor, S., Chamberlin, S. J., Chatterjee, S., Christy, B., ... & NANOGrav Collaboration. (2016). *The NANOGrav nine-year data set: limits on the isotropic stochastic gravitational wave background*. The Astrophysical Journal, 821(1), 13.
- [69] Guo, S. Y., Khlopov, M., Liu, X., Wu, L., Wu, Y., & Zhu, B. (2023). *Footprints of Axion-Like Particle in Pulsar Timing Array Data and JWST Observations*. arXiv preprint arXiv:2306.17022.
- [70] Zhao, W., Zhang, Y., You, X. P., & Zhu, Z. H. (2013). *Constraints of relic gravitational waves by pulsar timing arrays: Forecasts for the FAST and SKA projects*. Physical Review D, 87(12), 124012.
- [71] Gouttenoire, Y., Trifinopoulos, S., Valogiannis, G., & Vanvlasselaer, M. (2023). *Scrutinizing the Primordial Black Holes Interpretation of PTA Gravitational Waves and JWST Early Galaxies*. arXiv preprint arXiv:2307.01457.
- [72] Sasaki, M., Suyama, T., Tanaka, T., & Yokoyama, S. (2018). *Primordial black holes-perspectives in gravitational wave astronomy*. Classical and Quantum Gravity, 35(6), 063001.
- [73] Nakamura, T., Sasaki, M., Tanaka, T., & Thorne, K. S. (1997). *Gravitational waves from coalescing black hole MACHO binaries*. The Astrophysical Journal, 487(2), L139.
- [74] Quinlan, G. D., & Shapiro, S. L. (1988). *Star cluster collapse to a supermassive black hole: binaries and gravitational radiation*. In Proceedings of the 2nd Canadian Conference on General Relativity and Relativistic Astrophysics (pp. 335-338).
- [75] Mouri, H., & Taniguchi, Y. (2002). *Runaway merging of black holes: analytical constraint on the timescale*. The Astrophysical Journal, 566(1), L17.
- [76] Bird, S., Cholis, I., Muñoz, J. B., Ali-Haïmoud, Y., Kamionkowski, M., Kovetz, E. D., ... & Riess, A. G. (2016). *Did LIGO detect dark matter?*. Physical review letters, 116(20), 201301.
- [77] Atal, V., Blanco-Pillado, J. J., Sanglas, A., & Triantafyllou, N. (2022). *Constraining changes in the merger history of BH and PBH binaries with the stochastic gravitational wave background*. Physical Review D, 105(12), 123522.
- [78] Abbott, B. P., Abbott, R., Abbott, T. D., Abernathy, M. R., Acernese, F., Ackley, K., ... & Chakraborty, R. (2016). *GW150914: Implications for the stochastic gravitational-wave background from binary black holes*. Physical review letters, 116(13), 131102.
- [79] Abbott, B. P., Jawahar, S., Lockerbie, N. A., & Tokmakov, K. V. (2016). *LIGO Scientific Collaboration and Virgo Collaboration (2016) Directly comparing GW150914 with numerical solutions of Einstein's equations for binary black hole coalescence*. Physical Review D, 94 (6). ISSN 1550-2368, <http://dx.doi.org/10.1103/PhysRevD.94.064035>. PHYSICAL REVIEW D Phys Rev D, 94, 064035.
- [80] Ajith, P., Babak, S., Chen, Y., Hewitson, M., Krishnan, B., Sintes, A. M., ... & Thornburg, J. (2008). *Template bank for gravitational waveforms from coalescing binary black holes: Nonspinning binaries*. Physical Review D, 77(10), 104017.
- [81] Ajith, P., Hannam, M., Husa, S., Chen, Y., Brüggmann, B., Dorband, N., ... & Seiler, J. (2011). *Inspiral-merger-ringdown waveforms for black-hole binaries with nonprecessing spins*. Physical Review Letters, 106(24), 241101.
- [82] Ajith, P., Babak, S., Chen, Y., Hewitson, M., Krishnan, B., Sintes, A. M., ... & Thornburg, J. (2008). *Template bank for gravitational waveforms from coalescing binary black holes: Nonspinning binaries*. Physical Review D, 77(10), 104017.
- [83] Zhu, X. J., Howell, E., Regimbau, T., Blair, D., & Zhu, Z. H. (2011). *Stochastic gravitational wave background from coalescing binary black holes*. The Astrophysical Journal, 739(2), 86.
- [84] Khlopov, M. Y., Rubin, S. G., & Sakharov, A. S. (2002). *Strong primordial inhomogeneities and galaxy formation*. arXiv preprint astro-ph/0202505.
- [85] Khlopov, M. Y., Rubin, S. G., & Sakharov, A. S. (2005). *Primordial structure of massive black hole clusters*. Astroparticle Physics, 23(2), 265-277.
- [86] Khlopov, M. (2007, May). *Primordial nonlinear structures and massive black holes from early Universe*. In Journal of Physics: Conference Series (Vol. 66, No. 1, p. 012032). IOP Publishing.
- [87] Khlopov, M. Y. (2010). *Primordial black holes*. Research in Astronomy and Astrophysics, 10(6), 495.
- [88] Carr, Bernard J. "The Primordial black hole mass spectrum." (1975): 1-19.
- [89] N. Sanchez, A. Zichichi, *Current Topics in Astrofundamental Physics* edited by N. Sanchez (1997)
- [90] Green, A. M., & Liddle, A. R. (1997). *Constraints on the density perturbation spectrum from primordial black holes*. Physical Review D, 56(10), 6166.
- [91] Bhaumik, N., & Jain, R. K. (2020). *Primordial black holes dark matter from inflection point models of inflation and the effects of reheating*. Journal of Cosmology and Astroparticle Physics, 2020(01), 037.
- [92] Zhou, Z., Jiang, J., Cai, Y. F., Sasaki, M., & Pi, S. (2020). *Primordial black holes and gravitational waves from resonant amplification during inflation*. Physical Review D, 102(10), 103527.
- [93] Green, A. M., & Malik, K. A. (2001). *Primordial black hole production due to preheating*. Physical Review D, 64(2), 021301.
- [94] El Bourakadi, K., et al. "Primordial black holes and gravitational waves in teleparallel Gravity." The European Physical Journal C 82.9 (2022): 792.
- [95] Carr, B., Kohri, K., Sendouda, Y., & Yokoyama, J. I. (2021). *Constraints on primordial black holes*. Reports on Progress in Physics, 84(11), 116902.

- [96] Su, B. Y., Li, N., & Feng, L. (2023). *An inflation model for massive primordial black holes to interpret the JWST observations*. arXiv preprint arXiv:2306.05364.
- [97] De Luca, V., Franciolini, G., Pani, P., & Riotto, A. (2020). *Constraints on primordial black holes: the importance of accretion*. *Physical Review D*, 102(4), 043505.
- [98] De Luca, V., Franciolini, G., & Riotto, A. (2023). *Heavy Primordial Black Holes from Strongly Clustered Light Black Holes*. *Physical Review Letters*, 130(17), 171401.
- [99] Yuan, G. W., Lei, L., Wang, Y. Z., Wang, B., Wang, Y. Y., Chen, C., ... & Fan, Y. Z. (2023). *Rapidly growing primordial black holes as seeds of the massive high-redshift JWST Galaxies*. arXiv preprint arXiv:2303.09391.
- [100] Hoyle, F., & Narlikar, J. V. (1966). *On the formation of elliptical galaxies*. *Proceedings of the Royal Society of London. Series A. Mathematical and Physical Sciences*, 290(1421), 177-185.
- [101] Meszaros, P. (1975). *Primeval black holes and galaxy formation*. *Astronomy and Astrophysics*, 38, 5-13.
- [102] Carr, B. J., & Silk, J. (1983). *Can graininess in the early universe make galaxies?*. *Astrophysical Journal, Part 1 (ISSN 0004-637X)*, vol. 268, May 1, 1983, p. 1-16., 268, 1-16.
- [103] Carr, B. J., & Rees, M. J. (1984). *Can pregalactic objects generate galaxies?*. *Monthly Notices of the Royal Astronomical Society*, 206(4), 801-818.
- [104] Carr, B., & Silk, J. (2018). *Primordial black holes as generators of cosmic structures*. *Monthly Notices of the Royal Astronomical Society*, 478(3), 3756-3775.
- [105] Brockamp, M., Baumgardt, H., Britzen, S., & Zensus, A. (2016). *Unveiling Gargantua: A new search strategy for the most massive central cluster black holes*. *Astronomy & Astrophysics*, 585, A153.
- [106] Inoue, Y., & Kusenko, A. (2017). *New X-ray bound on density of primordial black holes*. *Journal of Cosmology and Astroparticle Physics*, 2017(10), 034.
- [107] Carr, B. J., & Sakellariadou, M. (1999). *Dynamical constraints on dark matter in compact objects*. *The Astrophysical Journal*, 516(1), 195.
- [108] Su, B. Y., Li, N., & Feng, L. (2023). *An inflation model for massive primordial black holes to interpret the JWST observations*. arXiv preprint arXiv:2306.05364.
- [109] Murgia, R., Scelfo, G., Viel, M., & Raccanelli, A. (2019). *Lyman- α forest constraints on primordial black holes as dark matter*. *Physical Review Letters*, 123(7), 071102.
- [110] Fan, X., Banados, E., & Simcoe, R. A. (2023). *Quasars and the intergalactic medium at cosmic dawn*. *Annual Review of Astronomy and Astrophysics*, 61, 373-426.
- [111] Banados, E., Venemans, B. P., Mazzucchelli, C., Farina, E. P., Walter, F., Wang, F., ... & Winters, J. M. (2018). *An 800-million-solar-mass black hole in a significantly neutral Universe at a redshift of 7.5*. *Nature*, 553(7689), 473-476.
- [112] Yang, J., Wang, F., Fan, X., Hennawi, J. F., Davies, F. B., Yue, M., ... & Walter, F. (2020). *Poniua 'ena: A Luminous $z=7.5$ Quasar Hosting a 1.5 Billion Solar Mass Black Hole*. *The Astrophysical Journal Letters*, 897(1), L14.
- [113] Wang, F., Fan, X., Yang, J., Mazzucchelli, C., Wu, X. B., Li, J. T., ... & Walter, F. (2021). *Revealing the accretion physics of supermassive black holes at redshift $z \sim 7$ with Chandra and infrared observations*. *The Astrophysical Journal*, 908(1), 53.
- [114] Farina, E. P., Schindler, J. T., Walter, F., Bañados, E., Davies, F. B., Decarli, R., ... & Onoue, M. (2022). *The x -shooter/alma sample of quasars in the epoch of reionization. ii. black hole masses, eddington ratios, and the formation of the first quasars*. *The Astrophysical Journal*, 941(2), 106.
- [115] Mazzucchelli, C., Bischetti, M., D'Odorico, V., Feruglio, C., Schindler, J. T., Onoue, M., ... & Zhu, Y. (2023). *XQR-30: Black hole masses and accretion rates of 42 $z \gtrsim 6$ quasars*. *Astronomy & Astrophysics*, 676, A71.
- [116] Yang, J., Wang, F., Fan, X., Hennawi, J. F., Barth, A. J., Bañados, E., ... & Zou, S. (2023). *A SPectroscopic Survey of Biased Halos in the Reionization Era (ASPIRE): A First Look at the Rest-frame Optical Spectra of $z > 6.5$ Quasars Using JWST*. *The Astrophysical Journal Letters*, 951(1), L5.
- [117] Inayoshi, K., Visbal, E., & Haiman, Z. (2020). *The assembly of the first massive black holes*. *Annual Review of Astronomy and Astrophysics*, 58, 27-97.
- [118] Volonteri, M., & Bellovary, J. (2012). *Black holes in the early Universe*. *Reports on Progress in Physics*, 75(12), 124901.
- [119] Curti, M., d'Eugenio, F., Carniani, S., Maiolino, R., Sandles, L., Witstok, J., ... & Wallace, I. E. (2023). *The chemical enrichment in the early Universe as probed by JWST via direct metallicity measurements at $z \sim 8$* . *Monthly Notices of the Royal Astronomical Society*, 518(1), 425-438.
- [120] Bouwens, R. J., Illingworth, G. D., González, V., Labbé, I., Franx, M., Conselice, C. J., ... & Zheng, W. (2010). *$z \sim 7$ Galaxy Candidates from NICMOS Observations Over the HDF-South and the CDF-South and HDF-North Goods Fields*. *The Astrophysical Journal*, 725(2), 1587.
- [121] Oesch, P. A., Brammer, G., Van Dokkum, P. G., Illingworth, G. D., Bouwens, R. J., Labbé, I., ... & Willner, S. P. (2016). *A remarkably luminous galaxy at $z = 11.1$ measured with Hubble Space Telescope grism spectroscopy*. *The Astrophysical Journal*, 819(2), 129.
- [122] Eisenstein, D. J., Willott, C., Alberts, S., Arribas, S., Bonaventura, N., Bunker, A. J., ... & Woodrum, C. (2023). *Overview of the JWST Advanced Deep Extragalactic Survey (JADES)*. arXiv preprint arXiv:2306.02465.
- [123] Bunker, A. J., Saxena, A., Cameron, A. J., Willott, C. J., Curtis-Lake, E., Jakobsen, P., ... & Whitler, L. (2023). *JADES NIRSpec Spectroscopy of GN-z11: Lyman- α emission and possible enhanced nitrogen abundance in $az = 10.60$ luminous galaxy*. *Astronomy & Astrophysics*, 677, A88.
- [124] Tacchella, S., Eisenstein, D. J., Hainline, K., Johnson, B. D., Baker, W. M., Helton, J. M., ... & Whitler, L. (2023). *JADES Imaging of GN-z11: revealing the morphology and environment of a luminous galaxy 430 Myr after the Big Bang*. *The Astrophysical Journal*, 952(1), 74.

- [125] Maiolino, R., Scholtz, J., Witstok, J., Carniani, S., D'Eugenio, F., de Graaff, A., ... & Sun, F. (2024). *A small and vigorous black hole in the early Universe*. *Nature*, 627(8002), 59-63.
- [126] Terao, K., Nagao, T., Onishi, K., Matsuoka, K., Akiyama, M., Matsuoka, Y., & Yamashita, T. (2022). *Multiline Assessment of Narrow-line Regions in $z \sim 3$ Radio Galaxies*. *The Astrophysical Journal*, 929(1), 51.
- [127] Le Fèvre, O., Lemaux, B. C., Nakajima, K., Schaerer, D., Talia, M., Zamorani, G., ... & Dunlop, J. (2019). *The VIMOS Ultra-Deep Survey: evidence for AGN feedback in galaxies with CIII- λ 1908 Å emission 10.8 to 12.5 Gyr ago*. *Astronomy & Astrophysics*, 625, A51.
- [128] Bondi, H. (1952). *On spherically symmetrical accretion*. *Monthly Notices of the Royal Astronomical Society*, 112(2), 195-204.
- [129] Hoyle, F., & Lyttleton, R. A. (1939, July). *The effect of interstellar matter on climatic variation*. In *Mathematical proceedings of the Cambridge philosophical society* (Vol. 35, No. 3, pp. 405-415). Cambridge University Press.
- [130] Bondi, H., & Hoyle, F. (1944). *On the mechanism of accretion by stars*. *Monthly Notices of the Royal Astronomical Society*, 104(5), 273-282.
- [131] Valentini, M., Murante, G., Borgani, S., Granato, G. L., Monaco, P., Brighenti, F., ... & Lapi, A. (2020). *Impact of AGN feedback on galaxies and their multiphase ISM across cosmic time*. *Monthly Notices of the Royal Astronomical Society*, 491(2), 2779-2807.
- [132] Eddington, A. S. (1979). *The internal constitution of the stars*. In *A Source Book in Astronomy and Astrophysics, 1900-1975* (pp. 281-290). Harvard University Press.